2015

Antarctic moss stress assessment based on chlorophyll content and leaf density retrieved from imaging spectroscopy data

Zbynek Malenovky
University of Wollongong, zbynek@uow.edu.au

Johanna Turnbull
University of Wollongong, jdt17@uowmail.edu.au

Arko Lucieer
University of Tasmania, arko.lucieer@utas.edu.au

Sharon A. Robinson
University of Wollongong, sharonr@uow.edu.au

Publication Details

Malenovky, Z., Turnbull, J. D., Lucieer, A. & Robinson, S. A. (2015). Antarctic moss stress assessment based on chlorophyll content and leaf density retrieved from imaging spectroscopy data. New Phytologist, 208 (2), 608-624.

Antarctic moss stress assessment based on chlorophyll content and leaf density retrieved from imaging spectroscopy data

Abstract

The health of several East Antarctic moss-beds is declining as liquid water availability is reduced due to recent environmental changes. Consequently, a noninvasive and spatially explicit method is needed to assess the vigour of mosses spread throughout rocky Antarctic landscapes. Here, we explore the possibility of using near-distance imaging spectroscopy for spatial assessment of moss-bed health. Turf chlorophyll a and b, water content and leaf density were selected as quantitative stress indicators. Reflectance of three dominant Antarctic mosses Bryum pseudotriquetrum, Ceratodon purpureus and Schistidium antarctici was measured during a drought-stress and recovery laboratory experiment and also with an imaging spectrometer outdoors on water-deficient (stressed) and well-watered (unstressed) moss test sites. The stress-indicating moss traits were derived from visible and near infrared turf reflectance using a nonlinear support vector regression. Laboratory estimates of chlorophyll content and leaf density were achieved with the lowest systematic/unsystematic root mean square errors of 38.0/235.2 nmol g−1 DW and 0.8/1.6 leaves mm−1, respectively. Subsequent combination of these indicators retrieved from field hyperspectral images produced small-scale maps indicating relative moss vigour. Once applied and validated on remotely sensed airborne spectral images, this methodology could provide quantitative maps suitable for long-term monitoring of Antarctic moss-bed health.

Disciplines

Medicine and Health Sciences | Social and Behavioral Sciences

Publication Details

Malenovky, Z., Turnbull, J. D., Lucieer, A. & Robinson, S. A. (2015). Antarctic moss stress assessment based on chlorophyll content and leaf density retrieved from imaging spectroscopy data. New Phytologist, 208 (2), 608-624.

Methods

Antarctic moss stress assessment based on chlorophyll content and leaf density retrieved from imaging spectroscopy data

Zbyněk Malenovský[1,2], Johanna D. Turnbull[1], Arko Lucieer[2], and Sharon A. Robinson[1]

[1] Centre for Sustainable Ecosystem Solutions, School of Biological Sciences, University of Wollongong, Northfields Avenue, Wollongong, NSW 2522, Australia

[2] Surveying and Spatial Sciences Group, School of Land and Food, University of Tasmania, Private Bag 76, TAS 7001 Hobart, Australia

Author for correspondence:
Zbyněk Malenovský
Centre for Sustainable Ecosystem Solutions, University of Wollongong,
Northfields Avenue, Wollongong, NSW 2522, Australia
tel: +61448936336, email: zbynek.malenovsky@gmail.com

Total word count (excluding summary, references, and legends): 6528
Summary: 198
Introduction: 903
Materials and methods: 3613
Results: 1191
Discussion: 714
Acknowledgements: 107
No. of Figures: 11 (Figs 1, 2, 3, 4, 5, 6, 8, 9, and 11 in colour)
No. of Tables: 1
No. of Supporting Information files: 4 (Fig. S1-S3; Table S1)

Summary

- The health of several East Antarctic moss-beds is declining as liquid water availability is reduced due to recent environmental changes. Consequently, a non-invasive and spatially explicit method is needed to assess the vigour of mosses spread throughout rocky Antarctic landscapes. Here, we explore the possibility of using near-distance imaging spectroscopy for spatial assessment of moss-bed health.
- Turf chlorophyll *a*+*b*, water content and leaf density were selected as quantitative stress indicators. Reflectance of three dominant Antarctic mosses *Bryum pseudotriquetrum*, *Ceratodon purpureus* and *Schistidium antarctici* was measured during a drought-stress and recovery laboratory experiment and also with an imaging spectrometer outdoors on water-deficient (stressed) and well-watered (unstressed) moss test sites. The stress-indicating moss traits were derived from visible and near infrared turf reflectance using a non-linear support vector regression.
- Laboratory estimates of chlorophyll content and leaf density were achieved with the lowest systematic/unsystematic root mean square errors of 38.0/235.2 nmol dwg^{-1} and 0.8/1.6 leaves mm^{-1}, respectively. Subsequent combination of these indicators retrieved from field hyperspectral images produced small-scale maps indicating relative moss vigour.
- Once applied and validated on remotely sensed airborne spectral images, this methodology could provide quantitative maps suitable for long-term monitoring of Antarctic moss-bed health.

Key words: stress imaging spectroscopy, hyperspectral remote sensing, moss chlorophyll content (Cab), turf water content (TWC), leaf density (LD), *Bryum pseudotriquetrum*, *Ceratodon purpureus*, *Schistidium antarctici*.

Introduction

Arctic polar regions are experiencing rapid and severe climatic shifts with major changes in the abundance, distribution, and phenology of plant species (MacDonald, 2010). Corresponding changes have already been documented in maritime Antarctica and the sub-Antarctic islands, where temperature changes have been particularly pronounced (Turner *et al.*, 2007). Less severe, but significant changes in air temperature, wind speed, and long-term fluctuations in concentration of stratospheric ozone have also been observed on the Antarctic continent (Turner *et al.*, 2005; Clarke *et al.*, 2008; Son *et al.*, 2010; Robinson & Erickson, 2014; Williamson *et al.*, 2014). Therefore, the Intergovernmental Panel on Climate Change recommended regular acquisitions and analyses of long-term Antarctic datasets (IPCC, 2007) and the Scientific Committee for Antarctic Research is proposing the establishment of an Antarctic Near-shore and Terrestrial Observing System (ANTOS) to provide baseline data for ecosystem health and to enable assessment of future changes.

Antarctic cryptogamic vegetation lacks vascular tissue and is poikilohydric, with plants only metabolically and photosynthetically active when hydrated (Schlensog *et al.*, 2013). Mosses and lichens that dominate the Antarctic vegetation are found in ice-free areas where sufficient summer snowmelt occurs (Wasley *et al.*, 2006). Around the coast, where ancient penguin colonies or recent nesting birds have provided nutrients, well-established moss-beds have developed (Wasley *et al.*, 2012). The Windmill Islands region of East Antarctica is one such area supporting some of the best-developed and most extensive moss ecosystems on the continent. However, since ice-free areas are also prime sites for polar stations and experience the largest visitor pressure in addition to the existing environmental stress, there is an urgent need to develop effective ways to measure and monitor the health of these ecosystems. Because mosses are sensitive to mechanical damage (i.e. trampling) and their growing season is short, the method needs to be non-invasive, rapid, and covering large moss-bed areas (i.e. spatially explicit). Given the unfavourable cold weather, a technique that allows data to be collected quickly and post processed later indoors is also preferable. An ideal solution would be an imaging remote sensing method that would allow fast spatial assessment of whole moss-beds, and thus enable repeated and standardized observations conducted under different climatic conditions of successive growing seasons.

A number of studies have demonstrated that remote sensing imaging spectroscopy, also referred to as hyperspectral remote sensing, can provide a qualitative description of vegetation (e.g. maps of plant functional types; Poulter *et al.*, 2011), but also quantitative estimates of plant biochemical and structural physiological traits (Malenovský *et al.*, 2009; Homolová *et al.*, 2013; Serbin *et al.*, 2014; Asner *et al.*, 2015). The special issue on imaging spectroscopy in Remote Sensing of Environment (Ustin & Schaepman, 2009) has shown various state-of-the-art techniques for bridging scaling gaps between foliar biochemical molecules and ecosystem canopies (Kokaly *et al.*, 2009). It provides insights into empirical methods for retrieving quantitative vegetation traits using optical vegetation indices and statistical functions (Ustin *et al.*, 2009), as well as physical inversion approaches based on coupled leaf and canopy radiative transfer models (Jacquemoud *et al.*, 2009; Schaepman *et al.*, 2009). This demonstrates an increasing capability of this scientific field towards spatially explicit quantitative characterisation of vegetation. Remote sensing estimates as leaf chlorophyll and water content or leaf area index (Hu *et al.*, 2004; Cheng *et al.*, 2006; Malenovský *et al.*, 2013) can parameterize and validate vegetation production models (e.g. yield predicting crop models; Clevers, 1997), but also indicate plant stress reactions (Zarco-Tejada *et al.*, 2002). Having standardised physical units, they are site and method independent. Moreover, the accuracy assessment of the estimates can be included in subsequent analyses (Demarty *et al.*, 2007).

The objective of this research is to test the hypothesis that the remotely sensed moss reflectance of visible and near infrared (VNIR) wavelengths (400–900 nm) can provide sufficiently accurate estimates of quantitative parameters indicating the physiological stress response (relative vigour) of Antarctic moss-beds to highly variable environmental changes. An acute stress load causes reorganisation of the moss pigment-bed, resulting in decline of leaf chlorophyll (Robinson *et al.*, 2005). Water deficiency (i.e. desiccation) triggers reduction of moss photosynthetic production and induces shape changes and geometrical re-arrangement (i.e. 'shrinking' and 'curling') of moss leaves (Zotz & Kahler, 2007). We observed that long-term stress slows moss growth, which results in shorter shoots with smaller leaves at higher density, whereas optimal growing conditions produce less dense and larger moss leaves. Therefore, the stress assessment approach proposed in this study has foundations in estimates of moss chlorophyll *a* and *b* content (Cab), turf water content (TWC) and leaf density (LD) retrieved from spectroscopy data of high spectral sampling and resolution (i.e. hyperspectral data). The method is intentionally based on quantitative bio-indicators, which ensures its transferability to other moss ecosystems along the Antarctic coast and to polar and alpine regions. A machine-learning algorithm, support vector regression, was parameterized and trained using laboratory-measured VNIR reflectance of moss and also continuum removal normalized reflectance to estimate Cab, TWC, and LD of three Antarctic moss species: *Bryum pseudotriquetrum*, *Ceratodon purpureus* and *Schistidium antarctici*. The successfully validated Cab and LD estimating algorithms were further applied to near-distance hyperspectral images of *S. antarctici* moss-beds acquired on the ground. Cab and LD maps were normalised and averaged to reveal the spatial pattern of actual relative moss vigour. This method can be applied to imaging spectroscopy data collected over Antarctic moss-beds with hyperspectral piloted or unmanned airborne systems and successively scaled up to satellite observations.

Materials and methods

Study area

The study was carried out in the vicinity of Australian Antarctic Casey station located in the Windmill Islands region, East Antarctica (66°17'S, 110°32'E; Fig. 1a). The ice-free habitats of this region support some of the most extensive and best-developed moss-beds on Continental Antarctica. The summer melt provides water sustaining populations of four bryophyte species including the endemic moss *Schistidium antarctici* (Cardot) L.I. Savicz & Smirnova, and two cosmopolitan species, *Bryum pseudotriquetrum* (Hedw.) Gaertn., Meyer & Scherb., and *Ceratodon purpureus* (Hedw.) Brid. The moss samples for laboratory experimental work were collected near Casey station, whilst the field hyperspectral data were acquired in natural moss ecosystems within Antarctic Specially Protected Area (ASPA) 135, located approximately 300 m southwest of the station (Fig. 1b).

Drought-stress rehydration experiment

Liquid water availability is a more important determinant of cryptogamic productivity in Antarctica than temperature (Kennedy, 1993; Schlensog *et al.*, 2013). Thus, a moss drought-stress rehydration experiment was designed and conducted in the Casey laboratory during the 2012–2013 summer season to establish a link between reflectance and stress-indicating biochemical and physical traits of moss turf (Lovelock & Robinson, 2002). Sampling included the three Antarctic moss species (*B. pseudotriquetrum*, *C. purpureus* and *S. antarctici*) and was designed to capture the existing natural variability in composition and content of moss foliar pigments. Turf sections (approximately 50 cm^2) of both visually red and green coloured moss turfs were collected from sites around the station on 26th December 2012 (n = 3 per species/colour except for green *C. purpureus* where n = 1). The 16 turf pieces were transferred to the laboratory and split in half (n = 32). Drought stress was applied to the first half, while the second half served as a stress-free control set. During clear days of the summer growth period the moss turf temperature reaches 20-30 °C (Bramley-Alves *et al.*, 2015). All samples were, therefore, kept in a plant growth cabinet with a constant temperature of 25 °C (the optimum for their photosynthetic activity), and 16 h light (photosynthetic flux density of 150 µmol photons m^{-2} s^{-1})/8 h dark. This low light intensity was applied to prevent any confounding high irradiation stress. To induce acute drought-stress, the first half of the samples was kept without water supply for six days after collection, whilst samples of the control half were soaked (completely saturated) with water every second day. From day 7, all samples were watered every second day until the end of the experiment on 25th January 2013 to observe drought stress recovery in the first half and growth under optimal conditions in the second half of samples (see examples in Fig. 2a). Every six days all samples were monitored for turf reflectance and total weight (a proxy of actual water content). Micro-photos were taken for assessment of shoot and leaf architectural changes and several shoot apices were collected from drought-stressed samples for later determination of pigment quantities. At the end of the experiment, samples were oven dried at 80°C to determine their dry mass.

A second independent dataset of 73 *S. antarctici* samples, which was collected and measured at Casey station in 1999, was used to validate relationships established during the 2013 drought-stress rehydration experiment. These samples were also used to establish the link between moss leaf density measurements and reflectance signatures. For detailed information of the 1999 sampling design see Robinson *et al.* (2005).

Laboratory spectral measurements of moss reflectance

Spectral measurements of moss samples during the drought-stress rehydration experiment were performed with an ASD HandHeld-2 (HH2) spectrometer (ASD Inc. & PANalytical, USA): wavelength range 325 and 1075 nm, spectral resolution about 1 nm, and the spectral band full width at half maximum (FWHM) about 3 nm. Since an optical integrating sphere was not available, the spectrometer was placed in a small dark chamber pointing downward at a zenith angle of 45°. Samples were illuminated with an external halogen Tungsten light source (power 50 W, field of view (FOV) about 24°) placed in nadir direction 45 cm from the sample and their reflected radiance was recorded from a distance of approximately 5 cm by the spectrometer optical fibres (FOV of 25°) (Fig. 2b). Six spectral measurements across each moss sample were recorded to account for turf spatial heterogeneity. Although microstructure of moss turf represents a near-Lambertian surface producing diffuse (i.e. hemispherically distributed) reflectance, samples for each measurement were rotated 45° clock-wise in order to compensate for any potential reflectance directional effect. The final sample reflectance was obtained as the mean of the six measured reflectance factors (ρ) computed as:

$$\rho = \frac{R_{sample} - R_{DC}}{R_{REF} - R_{DC}} \qquad \text{Eqn 1}$$

where R_{sample} is the radiance of the sample, R_{DC} is Dark Current radiance measured without any irradiation (sensor noise), and R_{REF} is radiance of a 99% reflective white reference (barium sulphate Spectralon panel). This protocol guaranteed that final reflectance is comparable with directional-hemispherical measurements obtained with an optical integrating sphere (Schaepman-Strub *et al.*, 2006).

The second validation dataset of moss reflectance between 200 and 900 nm was acquired in 1999 in an integrating sphere fitted to a scanning spectrophotometer GBC UV-Vis 918 (GBC, Dandenong, VIC, Australia) as described in Lovelock and Robinson (2002). Because the spectral datasets from 1999 and 2013 were acquired with two instruments of different spectral specifications, all measurements were spectrally unified to be compatible with field hyperspectral scans. The laboratory spectral datasets were resampled and convolved according to the actual spectral sampling, resolution, and FWHM of the outdoor imaging spectrometer observations (sensor technical specifications provided in field imaging spectroscopy section).

<u>Determination of chlorophyll content</u>

Several moss apices were cut from the top of drought-stressed samples after each spectral measurement in 2013. Samples were frozen at –80°C and transported to Australia for chlorophyll determination. There, they were freeze dried overnight

(Alpha 1-2 series freeze dryer, Fisher Bioblock Scientific, Illkirch, France) and homogenized for 2 minutes at 30 Hz in a tissue lyser (Retsch, Verder Group, Haan, Germany). Samples with a minimal dry weight of 8 mg were extracted in 600 μl of ethyl acetate/acetone (60% ETOAC and 40% acetone) with further homogenisation (2 min at 30 Hz), followed by the addition of 500 μl of milliQ water and centrifugation (5 min at 3600 g) (Dunn *et al.*, 2004; Förster *et al.*, 2011). Supernatant was diluted with 20% acetone and chlorophyll absorption peaks at 646.6, 663.6, and 750.0 nm were measured with a Shimadzu UV-visible spectrophotometer (Model 1601, Shimadzu, Kyoto, Japan). Chlorophyll *a* and chlorophyll *b* in nmol per gram of dry weight (Cab; nmol gdw^{-1}) were calculated using the equations published by Porra *et al.* (1989). Chlorophyll determination of 1999 samples followed a similar procedure (see Lovelock & Robinson, 2002).

<u>Moss water content and leaf density</u>

Moss turf water content (TWC; gH_2O gdw^{-1}), i.e. the difference between fresh and dry sample weights relative to a gram of dry turf weight, for both datasets was determined after oven drying (80°C) to a stable weight (see Robinson *et al.*, 2000).

Leaf density was only measured for *S. antarctici* samples in the 1999 validation dataset. Five randomly selected gametophytes from each sample were carefully dissected and the number of moss leaves in the top 3.5 mm was visually counted using a binocular microscope Leica Wild (Leica Microsystems, Gladesville, NSW, Australia). Mean leaf density per 1.0 mm of shoot length (LD; leaves mm^{-1}) was calculated according to Robinson *et al.* (2005). This time-consuming measurement was not repeated for samples from 2013. However, microscopic photos of each sample in natural colours were taken with a Dino-Lite AM 2111 digital microscope

(AnMo Electronics Corp., Taipei, Taiwan) on each sampling day to visually inspect shoot and leaf architectural changes during the experiment.

Field imaging spectroscopy

Two research plots of *c.* 10–15 m^2, colonised dominantly by *S. antarctici*, were chosen at ASPA 135 to demonstrate transferability of the approach developed in the laboratory to field near-distance hyperspectral images. The first plot, evaluated as a *dry* (exposed, water limited, and considerably stressed) moss-bed of lower vigour, was located at the top of a hill above the ASPA 135 fresh water lake (Fig. 1c). The second plot, representing a *wet* (lengthily snow covered, well watered, and less stressed) moss-bed of higher vigour, was positioned in a local terrain depression with water supply originating from snowmelt and possibly from infiltration of lake water located above (see Supporting Information Fig. S1).

The imaging spectroradiometer used for field near-distance hyperspectral observations (Ač *et al.*, 2009) was the Headwall Photonics Micro-Hyperspec VNIR scanner (Headwall Inc., Fitchburg, USA) attached to a computer-controlled rotating/tilting platform (Fig. 1d). The sensor unit was placed approximately 2.5 m above the ground on a single pole mounted to a geodetic tripod (Fig. 1c). The Micro-Hyperspec is a push-broom scanner, which collects light passing through a lens objective with an aperture of f/2.8 (FOV of 49.8°) and through a slit entrance of 25 µm. The spectral wavelengths are split by an aberration-corrected convex holographic diffraction grating and projected onto a charge-coupled device (CCD) matrix with a digital dynamic range of 12-bits and size of 1004 by 1004 pixel units. Each column of the CCD matrix records the projected spatial information, whilst each row records separate wavelengths between 361 and 961 nm. To build a hyperspectral image, the rotating/tilting platform moves the spectrometer anticlockwise in a horizontal direction with the predefined speed and photon integration time preserving the quadratic shape of image pixels. The CCD registers the captured light split into 324 (full spectral extent, FWHM of 4.12–4.67 nm) or 162 spectral bands (binning of two neighbouring spectral pixels as a single recording unit, FWHM of 4.75–5.25 nm). Every image row is placed next to the previous one, creating a hyperspectral image with 1004 across-track columns and as many along-track rows as defined by the operators (Fig. 1e).

To ensure a high signal-to-noise ratio and simultaneously prevent oversaturation of the CCD dynamic range, we applied spectral binning (162 bands) combined with an integration time of 40 milliseconds (ms) and collected oblique hyperspectral images (azimuth viewing angles of 44° and 60°) of the test sites at solar noon on the 10th and 30th of January 2013. The image of the *dry* site was acquired under full overcast conditions, while the *wet* site image was taken under a clear sky. A distance of about 3.5 m between the sensor and objects resulted in images of 3260 by 1004 pixels with varying across-track spatial resolution of less than 10 mm. The 12-bit spectral images were radiometrically calibrated into radiance (mW cm^{-2} sr^{-1}µm^{-1}) and transformed into relative hemispherical reflectance by applying an empirical line atmospheric correction as described in Lucieer *et al.* (2014). The short and long wavelengths with unstable signals (i.e. 361–495 and 849–961 nm) were truncated and a local mean filter with a moving window of 3 bands in the visible (VIS: 496–710 nm) and 7 bands in the near infrared (NIR: 710–848 nm) wavelengths was applied to the reflectance function of each pixel to remove residual random spectral noise. To assess image spectral quality, reflectance of four spatially homogeneous targets was acquired together with hyperspectral scans. Three reflectance signatures of three rocks with varying brightness at the *dry* site and a green moss turf at the *wet* site were measured with ASD HH2 from a distance of about 150 mm (i.e. from a circular footprint of 66.5 mm in diameter) and averaged as ground reference spectra. The targets were located on the hyperspectral images and their reflectance grids of 7x7 pixels (i.e. less than 70x70 mm) were separated and averaged as remotely sensed spectra. The coefficient of determination for a linear relationship (r^2), the root mean square error (RMSE), and the index of agreement (d) (see description below) were computed between reference and remotely sensed spectra to evaluate their similarities.

Modified triangular vegetation index and reflectance continuum removal

Optical vegetation indices (VI) are mathematical transformations of spectral reflectance designed to maximize their sensitivity towards particular biochemical or physical plant characteristics and simultaneously to minimize the confounding effects of other nearby surfaces (e.g. a negative spectral influence of bare soil surrounding or underneath a vegetation canopy) (Myneni *et al.*, 1995). In this study, we applied the modified triangular vegetation index 2 (MTVI2; Haboudane *et al.*, 2004) to detect photosynthetically active moss captured in hyperspectral images of both study sites. MTVI2 is as a successor of the triangular vegetation index (TVI; Broge & Leblanc, 2001) exploiting systematic changes in the area of the triangle drawn between the reflectance amplitudes at 550, 670, and 800 nm (i.e. ρ_{550}, ρ_{670}, and ρ_{800}):

$$\mathrm{MTVI2} = \frac{1.5\left[1.2\left(\rho_{800}-\rho_{550}\right)-2.5\left(\rho_{670}-\rho_{550}\right)\right]}{\sqrt{\left(2\rho_{800}+1\right)^2-\left(6\rho_{800}-5\sqrt{\rho_{670}}\right)-0.5}}. \qquad \text{Eqn 2}$$

When stressed by insufficient water availability and elevated solar (including ultraviolet) irradiation, moss canopies change from a healthy fluffy, green turf to a stress-resisting dense yellow-brown pack, and ultimately a desiccated black mat

(Robinson *et al.*, 2005; Clarke & Robinson, 2008; Turnbull & Robinson, 2009; Wasley *et al.*, 2012). Since these stress reactions are followed by changes in the reflectance function causing a decrease of MTVI2, we could apply the threshold of MTVI2 $\geq$ 0.25 to separate the photosynthetically active green moss from moss in this latest dormant stage together with lichens, bare soil, and rocks. The threshold of 0.25 was derived as a breakpoint of the MTVI2 frequency histograms of hyperspectral scans. It corresponds with our observation that high frequencies of low MTVI2 values indicate presence of rocks, bare soil, lichens, and desiccated black moss. The MTVI2 histograms of both hyperspectral scans are provided in Supporting Information Fig. S2.

The reflectance continuum removal (CR) transformation (Clark & Roush, 1984) has been applied in several studies to enhance and normalise the specific absorption features of certain vegetation foliar biochemical constituents (Broge & Leblanc, 2001; Curran *et al.*, 2001; Kokaly, 2001), including xanthophyll and chlorophyll pigments (Malenovský *et al.*, 2006; Kováč *et al.*, 2012; Kováč *et al.*, 2013). Similarly to Malenovský *et al.* (2013), we applied CR to reflectance of photosynthetically active moss between 650 and 720 nm to normalize and enhance modifications in the shape of the reflectance function that are induced by varying red light absorption due to changes in chlorophyll content. Secondly, we applied CR to the reflectance curve between 710 and 780 nm in order to capture and standardise systematic reflectance changes caused by differences in NIR photon scattering and absorbance among moss shoots and leaves (i.e. turf architectural modifications) emerging as a consequence of varying water content (Lovelock & Robinson, 2002). Principles of the CR transformation are depicted for examples of both a drought stressed and an unstressed

B. pseudotriquetrum spectrum in Fig. 3. The continuum removal is computed according to the equation:

$$\mathrm{CR}_{j\in\langle\lambda_1,\lambda_2\rangle}=\left|\left(\frac{\rho_j}{\rho_{ji}}\right)-1\right| \qquad \text{Eqn 3}$$

where ρ_j is the measured reflectance of a band j and ρ_{ji} is the reflectance of the same band linearly interpolated within the predefined wavelength interval of $\langle\lambda_1, \lambda_2\rangle$ (i.e. 650–720 nm or 710–780 nm) (Fig. 3).

Support vector regression and retrieval error assessment

Support vector regression (SVR) is a widely used machine learning technique belonging to the family of support vector machines (SVMs) and designed specifically for a function estimation (Smola & Schölkopf, 2004). SVMs are linear or nonlinear algorithms firmly grounded in the framework of statistical learning theory (Vapnik, 1998) that has been developed since the 1960s (Vapnik & Lerner, 1963). These methods use a training optimisation technique to construct a hyperplane or set of hyperplanes in a high- or infinite-dimensional space, which can separate feature-classes for classifications, or quantitative estimates for regressions. The SVR models, proposed originally by Drucker *et al.* (1997), were recently employed in numerous quantitative predictions of biochemical and structural parameters of oceanic and terrestrial vegetation ecosystems from spectral remote sensing observations (Camps-Valls *et al.*, 2006; Camps-Valls *et al.*, 2009; Tuia *et al.*, 2011; Pasolli *et al.*, 2012). In our study, we applied the epsilon-SVR learning machine based on the nonlinear Gaussian radial basis function (RBF) kernel (Vapnik, 1998) to estimate moss chlorophyll *a* and *b* content (Cab), turf water content (TWC) and leaf density (LD).

The RBF kernel for two samples x and x′, represented as feature vectors in an input space, is defined as:

$$\mathrm{RBF}(\mathrm{x}, \mathrm{x}') = \exp\left(-\frac{(\mathrm{x}-\mathrm{x}')^2}{2\sigma^2}\right), \quad \text{Eqn 4}$$

where $(\mathrm{x} - \mathrm{x}')^2$ is the squared Euclidean distance between the two feature vectors and σ is a free parameter related to the width parameter of the RBF kernel γ through:

$$\gamma = -\frac{1}{2\sigma^2}. \quad \text{Eqn 5}$$

We used the epsilon-SVR algorithm available in the C++ Library for Support Vector Machines (LIBSVM; Chih-Chung & Chih-Jen, 2011). All training inputs were scaled between zero and one, by assigning the mean of each set to zero and its standard deviation to one. To find the optimal regression model, we presented each epsilon-SVR with a training dataset containing either moss reflectance or CR reflectance values and applied a dual optimisation grid-search combined with a 5-fold cross-validation to identify the best values for the cost parameter *C* (i.e. a penalty parameter of the error term) and for the width parameter γ of the RBF kernel. The cross-validation prevents overfitting of the regression model. In 5-fold cross-validation, the training set is divided into five subsets of equal size and only one selected subset is used to test regression models obtained during the *C* and γ optimization performed on the remaining four subsets. The optimal parameters *C* and γ are selected based on a minimal mean square error (MSE). The SVR is then trained again with the most optimal *C* and γ to generate the best performing prediction model. Our Cab estimating SVR models were trained on: i) the reflectance of wavelengths influenced by photosynthetically active foliar pigments (496–719 nm), ii) the reflectance of the strong absorption wavelengths (648–719 nm) of chlorophyll *a* and *b*, and iii) the CR reflectance of spectral interval in ii) excluding the first and last bands that after the CR transformation give null values (i.e. 652–715 nm). For TWC and LD, the SVR machines were trained on: i) the reflectance of all available NIR wavelengths influenced by turf architecture and water content (708–848 nm), ii) the reflectance of a selected NIR interval (708–782 nm), which excludes redundant bands of a flat vegetation spectral response called the NIR plateau, and iii) the CR reflectance of the spectral interval in ii) without the first and last bands of null CR values (i.e. 711–778 nm). The optimal C and γ values and related MSEs of all trained SVRs are available in Supporting Information Table S1.

Once successfully trained, the SVR models were applied in a prediction mode on independent testing datasets to validate their accuracy and to assess suitability of tested spectral inputs. For Cab and TWC we used data of 2013 as the training datasets and data of 1999 as the testing dataset. Since LD was measured only in 1999, the input dataset was split into training (two-thirds, n = 49) and validation subsets (one-third, n = 24), while preserving the Gaussian distribution of both datasets. RMSE, including its systematic ($RMSE_S$) and unsystematic ($RMSE_U$) components, r^2, and d were calculated between measured and estimated values to assess the SVR prediction accuracy. Under the assumption of a one-to-one linear relationship between the number (N) of error-free observations (O) and predictions (P), Willmott (1981) postulated RMSE and its systematic and unsystematic components to be computed as:

$$\mathrm{RMSE} = \sqrt{\frac{\sum_{i=1}^{N}\left(\mathrm{P}_i - \mathrm{O}_i\right)^2}{\mathrm{N}}}, \qquad \text{Eqn 6}$$

$$\mathrm{RMSE_S} = \sqrt{\frac{\sum_{i=1}^{N}\left(\hat{\mathrm{P}}_i - \mathrm{O}_i\right)^2}{\mathrm{N}}}, \text{ and} \qquad \text{Eqn 7}$$

$$\mathrm{RMSE_U} = \sqrt{\frac{\sum_{i=1}^{N}\left(P_i - \hat{P}_i\right)^2}{N}}, \qquad \text{Eqn 8}$$

where $\hat{P}_i = a + bO_i$, and a and b are the coefficients of an ordinary least squares regression between O and P. The systematic and unsystematic components are related to the RMSE as follows:

$$\mathrm{RMSE} = \sqrt{\left(\mathrm{RMSE_S^2} + \mathrm{RMSE_U^2}\right)}. \qquad \text{Eqn 9}$$

The RMSE components offer a deeper error assessment of SVR retrieval methods. If $\mathrm{RMSE_S}$ prevails over $\mathrm{RMSE_U}$, it means that the retrieval errors originate from the predictive model and that this model will always yield systematically biased estimates. In the opposite situation, when the RMSE is composed mostly by the $\mathrm{RMSE_U}$, the model is as good as it can be and the retrieval inaccuracy originates from random measurement errors caused by limited precision and noise of the applied methods and devices. Finally, the index of agreement (d) complements the RMSE assessment and the coefficient of determination (r^2). It is defined as:

$$d = 1 - \left(\frac{\sum_{i=1}^{N}\left(P_i - O_i\right)^2}{\sum_{i=1}^{N}\left(\left|'P_i\right| - \left|'O_i\right|\right)^2}\right), \qquad \text{Eqn 10}$$

with $'P_i = P_i - \bar{O}$ and $'O_i = O_i - \bar{O}$. The index indicates the degree to which the observed deviations of the mean observations $\bar{O}$ correspond in magnitude and sign to the predicted deviations of $\bar{O}$. It is a dimensionless indicator gaining values between 0.0 and 1.0, where d = 1.0 signals perfect agreement between estimates and corresponding observations, whereas d = 0.0 denotes their complete mismatch (Willmott, 1981).

Spatial assessment of relative moss vigour

The ultimate goal is to develop a method for assessing actual moss health spatially and quantitatively from remotely sensed near-distance VNIR hyperspectral data. To fulfil this objective, the best performing SVRs were applied per-pixel on the hyperspectral images of the *dry* and *wet* moss sites, resulting in quantitative maps of Cab and LD. Spatial estimation of TWC could not be accomplished, because the strength of the TWC signal in NIR moss reflectance was insufficient to train a satisfactory performing SVR. To provide a single moss health indicator we merged the Cab and LD maps into a synthetic map of a relative vigour indicator (RVI). RVI was computed as the mean of Cab and inverted LD, both scaled between zero and the largest value measured in laboratory, i.e. Cab = 1500 nmol gdw^{-1} and LD = 15 leaves mm^{-1}. The final map represents relative vigour, where 100% indicates optimally growing healthy moss, and 0% indicates moss highly stressed by unfavourable environmental conditions. Ground-based imaging spectroscopy data and maps resulting from this study are publically available at the Australian Antarctic Data Centre (Malenovský *et al.*, 2015).

Results

Moss reflectance changes induced by water stress

The crucial changes in moss reflectance during the drought-stress rehydration experiment are demonstrated by three examples in Figures 4 to 6. At the beginning of the experiment *C. purpureus* (Fig. 4) was rather dry (indicated by the lack of water absorption at 900–1000 nm) and contained predominantly red pigments (denoted by reflectance at 550 nm (ρ_{550}) < reflectance at 625 nm (ρ_{625})) in small undeveloped and densely packed leaves (MTVI2 = 0.36). After growing for 6 days under optimal conditions with regular irrigation, this species produced new green leaves resulting in $\rho_{550} = \rho_{625}$, but without any significant change in the NIR region (besides increased water absorption at 900–1000 nm) (MTVI2 = 0.39). Over the next three weeks, it produced a canopy of larger leaves with higher Cab, reflecting more NIR light ($\rho_{550} > \rho_{625}$) (MTVI2 = 0.67). Similarly, *S. antarctici* (Fig. 5) was rather red coloured and dry at the start (MTVI2 = 0.26). Six days in the growth chamber without additional water supply (drought stress) did not trigger much change in foliar pigment quantity and composition, indicated by almost no change in the VIS wavelengths, but did induce architectural turf changes. As turf dried out, the leaves ceased photosynthesis (no chlorophyll fluorescence was detected) and curled up, which effectively enhanced leaf density per mm of shoot length. These changes allowed NIR photons to penetrate and to be absorbed deeper into the turf, which lowered turf NIR reflectance. The area of triangle delineated between ρ_{550}, ρ_{670}, and ρ_{800} became smaller (MTVI2 = 0.17) than the one measured after 21 days of regular watering (MTVI2 = 0.39), when fresh larger leaves full of chlorophyll stimulated a significant increase in ρ_{550} and ρ_{800} (Fig. 5). These spectral changes justify our use of the MTVI2 threshold as a separator of spectrally dark, desiccated, and photosynthetically inactive turf (together with soil and stones) from brighter, wet, and actively growing moss. Finally, *B. pseudotriquetrum* (Fig. 6) was moist and had green open leaves (i.e. $\rho_{550} > \rho_{625}$, high ρ_{NIR}, and MTVI2 = 0.92) when collected. The drought-stress treatment applied for 6 days caused similar spectral changes as seen for *S. antarctici* above, with ρ_{NIR} becoming strongly diminished by shoot shrinking and leaf curling due to the low TWC (MTVI2 = 0.49). The *B. pseudotriquetrum* canopy flourished during the following three weeks in optimal growing conditions, as demonstrated by the substantial increase in area above the reflectance curve between 650 and 715 nm due to a higher Cab, and also by an expanding area under the curve between 710 and 780 nm (MTVI2 = 1.46) caused by larger and less dense leaves at the top of the canopy.

Spectral estimation of turf chlorophyll, water content and leaf density

Unfortunately, about 40% of the drought-stress rehydration experiment samples had to be excluded either because the weight of collected apices was too low after drying for reliable Cab determination (less than 8 mg), or because desiccated moss turfs occasionally fell apart and their reflectance could not be properly measured. Despite these losses, Table 1 shows a sufficiently high coefficient of dispersion and an acceptable coefficient of variation (close to one) computed for 54 Cab training samples of all species from 2013. Both coefficients computed for TWC of the pilot species *S. antarctici* training dataset from 2013 indicate that the TWC variation and dispersion originated mainly from samples under drought stress. Although TWC variation was suboptimal, dispersion of TWC values appeared to be adequate, i.e. close to one (Poisson distribution). The same is true for the LD training data from 1999 (Table 1).

Because absorption of chlorophyll molecules *a* and *b* is species independent, the Cab estimating SVR was trained with inputs of all three species together. The SVR trained with reflectance of 496–719 nm systematically underestimated the Cab content (Fig. 7a). Estimates with $RMSE_S$ two-times larger than $RMSE_U$ suggest an insufficient performance of the model. The performance was significantly improved ($RMSE_S < RMSE_U$) after training the SVR with reflectance of specific chlorophyll absorption wavelengths between 648 and 719 nm (Fig. 7b). The best results were, however, obtained with the CR reflectance of the same spectral region (RMSE = 238.3 nmol dwg^{-1}, $r^2 = 0.54$, and d = 0.85) (Fig. 7c).

Unlike Cab, the estimation of TWC strongly depends on the turf (shoot) structural characteristics of each species (Stanton *et al.*, 2014) and must be performed per species. We attempted to train SVR for TWC estimation of *S. antarctici* using reflectance of two spectral intervals (708–848 and 708–782 nm) and CR reflectance of the latter interval. Validation results revealed that reflectance-based SVRs were unable to predict TWC, producing negative estimates in many cases. Although all TWC estimations of the CR-based SVR gained positive values, they were inaccurate and significantly different from the laboratory measurements (RMSE = 3.0 gH_2O gdw^{-1}, $r^2 = 0.01$, and d = 0.43). Finally, LD of *S. antarctici* was estimated with SVR models trained with the same spectral inputs as TWC. Fig. 7d,e,f shows that all three SVRs retrieved reasonable LD predictions (RMSE ≤ 2.3 leaves mm^{-1}, $RMSE_S < RMSE_U$, $r^2 \geq 0.35$, and d ≥ 0.78), but the best results were achieved with SVR based on reflectance between 708 and 782 nm (RMSE = 1.8 leaves mm^{-1}, $r^2 = 0.55$, and d = 0.86). These outcomes suggest that Cab and LD moss parameters are retrievable from VNIR reflectance with acceptable accuracy, whereas estimation of TWC is not feasible with the available VNIR wavelengths.

Maps of relative moss vigour

Before conducting the moss health assessment of *wet* and *dry* research sites, spectral quality of their field hyperspectral images was tested using four spatially homogeneous natural targets. Results provided in Supporting Information (Fig. S3) demonstrate that the reference and remotely sensed spectral signatures are in close agreement (RMSE ≤ 0.0156, $r^2 \geq 0.89$, and d ≥ 0.90), especially within the spectral range of 600–848 nm. This confirms that the radiometric and atmospheric corrections applied were effective and that retrievals will not be affected by errors originating from hyperspectral data processing.

Pixels of hyperspectral images with MTVI2 < 0.25 representing stones, soil, and/or desiccated moss were masked out and the best performing SVRs (Fig. 7c,e) were applied per pixel to estimate Cab and effective LD of photosynthetically active moss pixels (Fig. 8a,b and Fig. 9a,b). Subsequently, the relative moss vigour indicator was computed as the mean of Cab and LD maps scaled between zero and one (Fig. 8c and Fig. 9c). Visual comparison of the maps confirms our expectation that moss turf of the *wet* site has generally greater relative vigour than the *dry* site, caused by higher Cab and lower LD. The relative distribution of *dry* site Cab is shifted towards lower values when compared to the *wet* site (Fig. 10a,d), while the opposite trend is seen for LD (Fig. 10b,e). Although these results clearly depend on the actual spatial extent of photosynthetically active moss captured in each hyperspectral scan, the spatial patterns and assessments of the relative moss vigour (Fig. 10c,f) correspond well with our visual in-situ observations.

Discussion

Interpretation and validation of quantitative retrievals

The method described here allows spatial quantitative evaluation of moss vigour at sub-centimetre resolution over an area of several square metres, which represents a significant advance compared to the earlier laboratory-based sampling methods (Lovelock & Robinson, 2002; Robinson *et al.*, 2005; Schlensog *et al.*, 2013). However, traditional ground-sampling approaches are still crucial for calibration and accuracy assessment of this novel indirect method. While the laboratory validation of Cab and LD estimates confirmed that our SVR models with RMSE originating mainly from measurement inaccuracies ($RMSE_S < RMSE_U$) are robust predictors (Fig. 7c,e), TWC prediction appeared to be unfeasible. This was because the NIR spectral region used for TWC retrieval did not encompass wavelengths with sufficient water absorption (Curcio & Petty, 1951). The minor water absorption features centred around 970 and 1200 nm are more suitable for estimating canopy water content (Clevers *et al.*, 2010; Ollinger, 2011), but these wavelengths were either too noisy or unavailable in our spectral data.

Our observations indicate that LD can, to some extent, be used as an indirect measure of TWC. Physical and optical relationships between LD, TWC, and NIR reflectance are illustrated in Fig. 11. The top of a sufficiently watered moss canopy with expanded leaves reflects significantly more NIR light than a desiccated canopy. The shrunken shoots and curled leaves of dry moss (Fig. 6) allow photons to travel deeper inside the turf where they are absorbed (Fig. 11a,b). Zotz and Kahler (2007) observed the same phenomenon for canopies of the moss *Tortula ruralis*. Their fibre optic probe measuring photosynthetically active radiation revealed light penetration of *c.* 0.8 cm in a dry moss canopy (TWC 27%), whereas in fully hydrated moss turf (TWC 95%) light reached a depth of only 0.4 cm. Small leaves with high LD, typical in stress-impacted mosses, increase NIR light scattering and consequently also photon absorbance probability, which in turn decreases moss reflectance (Fig. 11c,d). Leaves contracted and curled by actual water shortage effectively enhance LD, which further amplifies these optical effects (Fig. 11e,f). Hence, physically and/or effectively high LD retrieved from moss turf NIR reflectance can be considered as a synthetic indicator of acute low TWC combined with a long-term environmental stress load. It must be noted that changing shoot density also affects NIR reflectance independently from LD and occurrence of curling. Thus, a dedicated experiment investigating architectural canopy changes caused by desiccation of different moss species is required to confirm this conclusion and to investigate species-specific relations.

Finally, despite the successful validation of hyperspectral images (Fig. S3), the Cab and LD maps should be still compared with in-situ observations and laboratory measurements. Although the SVR models proved to be robust, limited variation in our training datasets contributes to high $RMSE_U$ (Fig. 7) and potentially causes inaccurate estimates of underrepresented Cab and LD values. Consequently, SVRs re-trained on extended datasets of increased variation might provide more accurate results with lower $RMSE_U$.

Method expansion and remote sensing application

Although only two stress indicators were combined in this study, more quantitative predictors could be incorporated in future moss vigour assessments. For example, green and red moss reflectance (i.e. wavelengths around 530 and 600 nm) can be used to reveal the content of xanthophyll and anthocyanin pigments (Francis, 1982; Gilmore & Yamamoto, 1991) indicating the level of photoprotection required by moss in response to solar irradiation stress (Gamon & Surfus, 1999; Kováč *et al.*, 2013). Since microhabitat light and moisture gradients also influence moss photosynthetic traits (Waite & Sack, 2010; Bramley-Alves *et al.*, 2015), certain stress-indicative photosynthetic parameters (e.g. non-photosynthetic quenching or light use efficiency) measured remotely from a distance of several meters using laser-induced chlorophyll fluorescence transient (LIFT) techniques (Kolber *et al.*, 2005; Pieruschka *et al.*, 2014) could also be included to complement the monitoring approach presented here.

By scaling up moss sample-based laboratory spectroscopy measurements to field hyperspectral scans, our study paves the way for future imaging spectroscopy of entire moss-beds sensed from piloted or unmanned aircraft systems (Lucieer *et al.*, 2014; Turner *et al.*, 2014). Yet, to fully address scientific questions related to the impact of a changing Antarctic climate on the dominant cryptogamic vegetation, local ground and airborne surveys need to be scaled further to regional satellite observations of low spatial, but high temporal resolutions.

Acknowledgements

This study was funded by Discovery grant DP110101714 from the Australian Research Council and Antarctic Science Grant no. 4046. The authors thank Anna Nydahl and Jessica Bramley-Alves for their indispensable field and laboratory assistance, Dr Catherine E. Lovelock for providing the moss dataset collected at Casey in 1999, Tony Veness and Darren Turner for technical assistance with the hyperspectral scanning equipment, and all participants of the Casey station Australian Antarctic expedition 2012-2013 for their genuine help. Authors are thankful for the constructive comments of anonymous reviewers that strengthened the scientific quality of the manuscript. Finally, the Australian Antarctic Division is acknowledged for field and logistic support.

References

Ač A, Malenovský Z, Hanuš J, Tomášková I, Urban O, Marek MV. 2009. Near-distance imaging spectroscopy investigating chlorophyll fluorescence and photosynthetic activity of grassland in the daily course. *Functional Plant Biology* **36**: 1006-1015.

Asner GP, Martin RE, Anderson CB, Knapp DE. 2015. Quantifying forest canopy traits: Imaging spectroscopy versus field survey. *Remote Sensing of Environment* **158**: 15-27.

Bramley-Alves J, Wanek W, French K, Robinson SA. 2015. Moss δ13C: an accurate proxy for past water environments in polar regions. *Global Change Biology* **21**: 2454-2464.

Broge NH, Leblanc E. 2001. Comparing prediction power and stability of broadband and hyperspectral vegetation indices for estimation of green leaf area index and canopy chlorophyll density. *Remote Sensing of Environment* **76**: 156-172.

Camps-Valls G, Bruzzone L, Rojo-Alvarez JL, Melgani F. 2006. Robust support vector regression for biophysical variable estimation from remotely sensed images. *Geoscience and Remote Sensing Letters, IEEE* **3**: 339-343.

Camps-Valls G, Munoz-Mari J, Gomez-Chova L, Richter K, Calpe-Maravilla J. 2009. Biophysical Parameter Estimation With a Semisupervised Support Vector Machine. *Geoscience and Remote Sensing Letters, IEEE* **6**: 248-252.

Cheng Y-B, Zarco-Tejada PJ, Riaño D, Rueda CA, Ustin SL. 2006. Estimating vegetation water content with hyperspectral data for different canopy scenarios: Relationships between AVIRIS and MODIS indexes. *Remote Sensing of Environment* **105**: 354-366.

Chih-Chung C, Chih-Jen L. 2011. LIBSVM: A library for support vector machines. *ACM Trans. Intell. Syst. Technol.* **2**: 1-27.

Clark RN, Roush TL. 1984. Reflectance spectroscopy: Quantitative analysis techniques for remote sensing applications. *Journal of Geophysical Research: Solid Earth* **89**: 6329-6340.

Clarke LJ, Ayre DJ, Robinson SA. 2008. Somatic mutation and the Antarctic ozone hole. *Journal of Ecology* **96**: 378-385.

Clarke LJ, Robinson SA. 2008. Cell wall-bound ultraviolet-screening compounds explain the high ultraviolet tolerance of the Antarctic moss, *Ceratodon purpureus*. *New Phytologist* **179**: 776-783.

Clevers JGPW. 1997. A simplified approach for yield prediction of sugar beet based on optical remote sensing data. *Remote Sensing of Environment* **61**: 221-228.

Clevers JGPW, Kooistra L, Schaepman ME. 2010. Estimating canopy water content using hyperspectral remote sensing data. *International Journal of Applied Earth Observation and Geoinformation* **12**: 119-125.

Curcio JA, Petty CC. 1951. The near infrared absorption spectrum of liquid water. *Journal of the Optical Society of America* **41**: 302-302.

Curran PJ, Dungan JL, Peterson DL. 2001. Estimating the foliar biochemical concentration of leaves with reflectance spectrometry: Testing the Kokaly and Clark methodologies. *Remote Sensing of Environment* **76**: 349-359.

Demarty J, Chevallier F, Friend AD, Viovy N, Piao S, Ciais P. 2007. Assimilation of global MODIS leaf area index retrievals within a terrestrial biosphere model. *Geophysical Research Letters* **34**: L15402.

Drucker H, Burges CJC, Kaufman L, Smola AJ, Vapnik V 1997. Support Vector Regression Machines. *Advances in Neural Information Processing Systems 9*: MIT Press. 155-161.

Dunn JL, Turnbull JD, Robinson SA. 2004. Comparison of solvent regimes for the extraction of photosynthetic pigments from leaves of higher plants. *Functional Plant Biology* **31**: 195-202.

Förster B, Pogson BJ, Osmond CB. 2011. Lutein from deepoxidation of lutein epoxide replaces zeaxanthin to sustain an enhanced capacity for nonphotochemical chlorophyll fluorescence quenching in avocado shade leaves in the dark. *Plant Physiology* **156**: 393-403.

Francis FJ 1982. Analysis of anthocyanins. In: Markakis P ed. *Anthocyanins as food colours*. New York: Academic Press, 181–207.

Gamon JA, Surfus JS. 1999. Assessing leaf pigment content and activity with a reflectometer. *New Phytologist* **143**: 105-117.

Gilmore AM, Yamamoto HY. 1991. Resolution of lutein and zeaxanthin using a non-endcapped, lightly carbon-loaded C_{18} high-performance liquid chromatographic column. *Journal of Chromatography* **543**: 137-145.

Haboudane D, Miller JR, Pattey E, Zarco-Tejada PJ, Strachan IB. 2004. Hyperspectral vegetation indices and novel algorithms for predicting green LAI of crop canopies: Modeling and validation in the context of precision agriculture. *Remote Sensing of Environment* **90**: 337-352.

Homolová L, Malenovsky Z, Schaepman ME, García-Santos G, Clevers JGPW. 2013. Review of optical-based remote sensing for plant trait mapping. *Ecological Complexity* **15**: 1-16.

Hu B, Qian S-E, Haboudane D, Miller JR, Hollinger AB, Tremblay N, Pattey E. 2004. Retrieval of crop chlorophyll content and leaf area index from decompressed hyperspectral data: the effects of data compression. *Remote Sensing of Environment* **92**: 139-152.

IPCC. 2007. Anisimov OA, Vaughan DG, Callaghan TV, Furgal C, Marchant H, Prowse TD, Vilhjálmsson H, Walsh JE, eds. *Climate Change 2007: Polar regions (Arctic and Antarctic) Impacts, Adaptation and Vulnerability.*

Contribution of Working Group II to the Fourth Assessment Report of the Intergovernmental Panel on Climate Change. Cambridge, UK & New York, NY, USA: Cambridge University Press.

Jacquemoud S, Verhoef W, Baret F, Bacour C, Zarco-Tejada PJ, Asner GP, François C, Ustin SL. 2009. PROSPECT & SAIL models: A review of use for vegetation characterization. *Remote Sensing of Environment* **113** S56-S66.

Kennedy AD. 1993. Water as a limiting factor in the Antarctic terrestrial environment: A biogeographical synthesis. *Arctic and Alpine Research* **25**: 308-315.

Kokaly RF. 2001. Investigating a physical basis for spectroscopic estimates of leaf nitrogen concentration. *Remote Sensing of Environment* **75**: 153-161.

Kokaly RF, Asner GP, Ollinger SV, Martin ME, Wessman CA. 2009. Characterizing canopy biochemistry from imaging spectroscopy and its application to ecosystem studies. *Remote Sensing of Environment* **113**: S78-S91.

Kolber Z, Klimov D, Ananyev G, Rascher U, Berry J, Osmond B. 2005. Measuring photosynthetic parameters at a distance: laser induced fluorescence transient (LIFT) method for remote measurements of photosynthesis in terrestrial vegetation. *Photosynthesis Research* **84**: 121-129.

Kováč D, M. N, Malenovský Z, Štorch M, Špunda V, Urban O. 2012. Reflectance continuum removal spectral index tracking the xanthophyll cycle photoprotective reactions in Norway spruce needles. *Functional Plant Biology* **39**: 987-998.

Kováč D, Malenovský Z, Urban O, Špunda V, Kalina J, Ač A, Kaplan V, Hanuš J. 2013. Response of green reflectance continuum removal index to xanthophyll de-epoxidation cycle in Norway spruce needles. *Journal of Experimental Botany* **64**: 1817-1827.

Lovelock CE, Robinson SA. 2002. Surface reflectance properties of Antarctic moss and their relationship to plant species, pigment composition and photosynthetic function. *Plant, Cell & Environment* **25**: 1239-1250.

Lucieer A, Malenovský Z, Veness T, Wallace L. 2014. HyperUAS-imaging spectroscopy from a multirotor unmanned aircraft system. *Journal of Field Robotics* **31**: 571-590.

MacDonald GM. 2010. Global warming and the Arctic: a new world beyond the reach of the Grinnellian niche? *The Journal of Experimental Biology* **213**: 855-861.

Malenovský Z, Homolová L, Zurita-Milla R, Lukeš P, Kaplan V, Hanuš J, Gastellu-Etchegorry J-P, Schaepman ME. 2013. Retrieval of spruce leaf chlorophyll content from airborne image data using continuum removal and radiative transfer. *Remote Sensing of Environment* **131**: 85-102.

Malenovský Z, Lucieer A, Robinson SA, Turnbull JD, Nydahl A. 2015. Ground-based imaging spectroscopy data for estimation of Antarctic moss relative vigour from remotely sensed chlorophyll content and leaf density at ASPA 135. *Australian Antarctic Data Centre*: doi: 10.4225/15/555C1DB80CB70.

Malenovský Z, Mishra KB, Zemek F, Rascher U, Nedbal L. 2009. Scientific and technical challenges in remote sensing of plant canopy reflectance and fluorescence. *Journal of Experimental Botany* **60**: 2987-3004.

Malenovský Z, Ufer C, Lhotáková Z, Clevers JGPW, Schaepman ME, Albrechtová J, Cudlín P. 2006. A new hyperspectral index for chlorophyll estimation of a forest canopy: Area under curve normalised to maximal band depth between 650-725 nm *EARSeL eProceedings* **5**: 161-172.

Myneni RB, Hall FG, Sellers PJ, Marshak AL. 1995. The interpretation of spectral vegetation indexes. *IEEE Transactions on Geoscience and Remote Sensing* **33**: 481-486.

Ollinger SV. 2011. Sources of variability in canopy reflectance and the convergent properties of plants. *New Phytologist* **189**: 375-394.

Pasolli E, Melgani F, Alajlan N, Bazi Y. 2012. Active Learning Methods for Biophysical Parameter Estimation. *IEEE Transactions on Geoscience and Remote Sensing* **50**: 4071-4084.

Pieruschka R, Albrecht H, Muller O, Berry JA, Klimov D, Kolber ZS, Malenovský Z, Rascher U. 2014. Daily and seasonal dynamics of remotely sensed photosynthetic efficiency in tree canopies. *Tree Physiology* **34**: 674-685.

Porra RJ, Thompson WA, Kriedemann PE. 1989. Determination of accurate extinction coefficients and simultaneous equations for assaying chlorophylls *a* and *b* extracted with four different solvents: verification of the concentration of chlorophyll standards by atomic absorption spectroscopy. *Biochimica et Biophysica Acta* **975**: 384-394.

Poulter B, Ciais P, Hodson E, Lischke H, Maignan F, Plummer S, Zimmermann NE. 2011. Plant functional type mapping for earth system models. *Geoscientific Model Development* **4**: 993-1010.

Robinson SA, Erickson DJ. 2014. Not just about sunburn – the ozone hole's profound effect on climate has significant implications for Southern Hemisphere ecosystems. *Global Change Biology* **21**: 515-527.

Robinson SA, Turnbull JD, Lovelock CE. 2005. Impact of changes in natural ultraviolet radiation on pigment composition, physiological and morphological characteristics of the Antarctic moss, *Grimmia antarctici*. *Global Change Biology* **11**: 476-489.

Robinson SA, Wasley J, Popp M, Lovelock CE. 2000. Desiccation tolerance of three moss species from continental Antarctica. *Australian Journal of Plant Physiology* **27**: 379-388.

Schaepman ME, Ustin SL, Plaza AJ, Painter TH, Verrelst J, Liang S. 2009. Earth system science related imaging spectroscopy - An assessment. *Remote Sensing of Environment* **113**: S123-S137.

Schaepman-Strub G, Schaepman ME, Painter TH, Dangel S, Martonchik JV. 2006. Reflectance quantities in optical remote sensing—Definitions and case studies. *Remote Sensing of Environment* **103**: 27-42.

Schlensog M, Green TGA, Schroeter B. 2013. Life form and water source interact to determine active time and environment in cryptogams: an example from the maritime Antarctic. *Oecologia* **173**: 59-72.

Serbin SP, Singh A, McNeil BE, Kingdon CC, Townsend PA. 2014. Spectroscopic determination of leaf morphological and biochemical traits for northern temperate and boreal tree species. *Ecological Applications* **24**: 1651-1669.

Smola AJ, Schölkopf BH. 2004. A tutorial on support vector regression. *Statistics and Computing* **14**: 199-222.

Son SW, Gerber EP, Perlwitz J, Polvani LM, Gillett NP, Seo KH, Eyring V, Shepherd TG, Waugh D, Akiyoshi H, et al. 2010. Impact of stratospheric ozone on Southern Hemisphere circulation change: A multimodel assessment. *Journal of Geophysical Research: Atmospheres* **115**: D00M07.

Stanton DE, Merlin M, Bryant G, Ball MC. 2014. Water redistribution determines photosynthetic responses to warming and drying in two polar mosses. *Functional Plant Biology* **41**: 178-186.

Tuia D, Verrelst J, Alonso L, Perez-Cruz F, Camps-Valls G. 2011. Multioutput Support Vector Regression for Remote Sensing Biophysical Parameter Estimation. *Geoscience and Remote Sensing Letters, IEEE* **8**: 804-808.

Turnbull JD, Robinson SA. 2009. Accumulation of DNA damage in Antarctic mosses: correlations with ultraviolet-B radiation, temperature and turf water content vary among species. *Global Change Biology* **15**: 319-329.

Turner D, Lucieer A, Malenovský Z, King D, Robinson S. 2014. Spatial co-registration of ultra-high resolution visible, multispectral and thermal images acquired with a micro-UAV over Antarctic moss beds. *Remote Sensing* **6**: 4003-4024.

Turner J, Colwell SR, Marshall GJ, Lachlan-Cope TA, Carleton AM, Jones PD, Lagun V, Reid PA, Iagovkina S. 2005. Antarctic climate change during the last 50 years. *International Journal of Climatology* **25**: 279-294.

Turner J, Overland JE, Walsh JE. 2007. An Arctic and Antarctic perspective on recent climate change. *International Journal of Climatology* **27**: 277-293.

Ustin SL, Gitelson AA, Jacquemoud S, Schaepman M, Asner GP, Gamon JA, Zarco-Tejada P. 2009. Retrieval of foliar information about plant pigment systems from high resolution spectroscopy. *Remote Sensing of Environment* **113**: S67-S77.

Ustin SL, Schaepman ME. 2009. Imaging spectroscopy special issue. *Remote Sensing of Environment* **113**: S1.

Vapnik NV. 1998. *Statistical Learning Theory*. New York: Wiley-Interscience.

Vapnik NV, Lerner A. 1963. Pattern Recognition using Generalized Portrait Method. *Automation and Remote Control* **24**: 774-780.

Waite M, Sack L. 2010. How does moss photosynthesis relate to leaf and canopy structure? Trait relationships for 10 Hawaiian species of contrasting light habitats. *New Phytologist* **185**: 156-172.

Wasley J, Robinson SA, Lovelock CE, Popp M. 2006. Some like it wet — biological characteristics underpinning tolerance of extreme water stress events in Antarctic bryophytes. *Functional Plant Biology* **33**: 443-455.

Wasley J, Robinson SA, Turnbull JD, King DH, Wanek W, Popp M. 2012. Bryophyte species composition over moisture gradients in the Windmill Islands, East Antarctica: Development of a baseline for monitoring climate change impacts. *Biodiversity* **13**: 257-264.

Williamson CE, Zepp RG, Lucas RM, Madronich S, Austin AT, Ballare CL, Norval M, Sulzberger B, Bais AF, McKenzie RL, et al. 2014. Solar ultraviolet radiation in a changing climate. *Nature Clim. Change* **4**: 434-441.

Willmott CJ. 1981. On the validation of models. *Physical Geography* **2**: 184-194.

Zarco-Tejada PJ, Miller JR, Mohammed GH, Noland TL, Sampson PH. 2002. Vegetation stress detection through chlorophyll a + b estimation and fluorescence effects on hyperspectral imagery. *J. Environ. Qual.* **31**: 1433-1441.

Zotz G, Kahler H. 2007. A moss “canopy” – Small-scale differences in microclimate and physiological traits in *Tortula ruralis*. *Flora - Morphology, Distribution, Functional Ecology of Plants* **202**: 661-666.

Supporting Information

Fig. S1 Illustration of *dry* and *wet* research plots at the Antarctic Specially Protected Area 135.

Fig. S2 Establishment of the modified triangular vegetation index 2 (MTVI2) threshold.

Fig. S3 Spectral quality validation of ground-based hyperspectral images acquired at both plots.

Table S1 Optimised input parameters and mean square errors of support vector regressions.

Tables

Table 1 Statistical description of chlorophyll *a* and *b* (Cab) and turf water content (TWC) for moss training samples (*C. purpureus*, *S. antarctici*, *B. pseudotriquetrum*) from 2013 and leaf density (LD) of 1999 *S. antarctici* training input samples.

Variable	*Species*	*n*	*Treatment*	*Mean*	*Std. Dev.*	*Coef. of Var.*[1]	*Coef. of Disp.*[2]
Cab – 2013 [nmol gdw^{-1}]	*C. purpureus*	19	DRY[3]	386.8	420.0	1.09	456.0
	S. antarctici	19	DRY	278.7	266.7	0.96	255.2
	B. pseudotriquetrum	16	DRY	549.5	309.5	0.56	174.3
	Total	*54*	*All*	*397.0*	*351.0*	*0.88*	*310.5*
TWC – 2013 [gH_2O gdw^{-1}]	*S. antarctici*	19	DRY	3.77	2.23	0.59	1.32
		19	WET[4]	5.75	1.49	0.26	0.39
		38	*Both*[5]	*4.79*	*2.11*	*0.44*	*0.93*
LD – 1999 [leaves mm^{-1}]	*S. antarctici*	49	N/A[6]	8.62	2.60	0.30	0.78

[1] Coefficient of Variation ~ Standard Deviation-to-Mean ratio (<1 ~ low variation, ≥1~ high variation)
[2] Coefficient of Dispersion ~ Variance-to-Mean ratio (0 ~ not dispersed, <1 ~ under-dispersed, ≥1 ~ well-dispersed)
[3] DRY treatment ~ sampled moss was kept for 6 days without water supply and then regularly irrigated.
[4] WET treatment ~ sampled moss was irrigated regularly during whole experiment.
[5] Both ~ DRY and WET treatments merged together.
[6] N/A ~ Not Applicable.

Figure legends

Fig.1

Geographical location of Antarctic Specially Protected Area (ASPA) 135 study sites close to the Australian Antarctic station Casey (a, b); the ground-based hyperspectral instrumentation in field (at the *dry* test site) (c); the Micro-Hyperspec imaging spectroradiometer (Headwall Inc., Fitchburg, USA) mounted on rotation and tilt platform (d); and a false-coloured near-distance hyperspectral image of a *Schistidium antarctici* moss bed at the *dry* test site (e). Red colour indicates photosynthetically active mosses, whereas grey and black colours represent rocks, bare soil, lichens, and desiccated black turf.

Fig. 2

Examples of laboratory drought-stress rehydration experiment samples of the three Antarctic moss species (*Ceratodon purpureus*, *Bryum pseudotriquetrum* and *Schistidium antarctici*) collected on 26 December 2012 (a). Half of the samples serving as controls were kept in optimal growing conditions and irrigated during the whole experiment (see example of red-coloured *C. purpureus*; blue tap icon symbolises regular irrigation every 2nd day), while the other half was kept without water until 1 December 2013 and then irrigated regularly until the end of the experiment on 25 January 2013 (see examples of green *B. pseudotriquetrum* and red-coloured *S. antarctici*; red crossed tap icon symbolises water-stress). Reflectance of all moss samples was measured every 6th day in a dark chamber with an ASD HandHeld-2 (HH2) spectrometer (ASD Inc. & PANalytical, Boulder, USA) coupled with a halogen tungsten irradiation light source (b).

Fig. 3

Mathematical explanation of the continuum removal (CR) transformation for spectral ranges of 650–715 and 710–780 nm, demonstrated on reflectance functions of a water-stressed and an unstressed *Bryum pseudotriquetrum* (a). Linearly interpolated values (ρ_l) are first computed for the given spectral intervals (dotted lines) and then applied per wavelength to normalize the original reflectance (ρ). The absolute value of this ratio subtracted from one results in the continuum removed (CR) reflectance of both spectral intervals: 650–715 nm (b) and 710–780 nm (c).

Fig. 4

Reflectance signatures and corresponding micro-photographs of *Ceratodon purpureus* collected and measured on 26 December 2012 (MTVI2 = 0.36), kept in optimal growing conditions (sufficiently irrigated) and re-measured on 1 January 2013 (MTVI2 = 0.39) and 25 January 2013 (MTVI2 = 0.67). The green background highlights the spectral range influenced mainly by actual composition and amount of foliar pigments, whereas the blue background indicates the spectral range influenced mainly by effective turf foliar density and actual turf water content.

Fig. 5

Reflectance signatures and corresponding micro-photographs of *Schistidium antarctici* collected and measured on 26 December 2012 (MTVI2 = 0.26), kept in a growth chamber without water and re-measured on 1 January 2013 (MTVI2 = 0.17), then rehydrated (sufficiently irrigated) and measured again on 25 January 2013 (MTVI2 = 0.39). Dashed lines delineating triangles between reflectance amplitudes at

550, 670 and 800 nm indicate increase in the area inside of the triangle with decreasing stress load. Declining MTVI2, caused by shrinking and curling of leaves indicates low water content on 1 January 2013. Green and blue backgrounds are explained in Fig. 4.

Fig. 6

Reflectance signatures and corresponding microscopic photographs of *Bryum pseudotriquetrum* collected and measured on 26 December 2012 (MTVI2 = 0.92), kept in a growth chamber without water and re-measured on 1 January 2013 (MTVI2 = 0.49), and then rehydrated and measured again on 25 January 2013 (MTVI2 = 1.46). Dotted lines denote spectral regions used for the continuum removal transformation. They show that both areas under the curve at 650–715 nm and at 710–780 nm increase as the stress load decreases and as the moss turf produces more chlorophyll and leaves open up. Declining MTVI2, caused by shrinking and curling of leaves and shoots, indicates low water content on 1 January 2013. Green and blue backgrounds are explained in Fig. 4.

Fig. 7

Accuracy assessment of chlorophyll *a+b* content (Cab) and mean leaf density (LD) estimates from *Schistidium antarctici* spectral measurements. Cab was estimated by support vector regression from samples collected in 1999 (n = 80) using their reflectance between 496 and 719 nm (SVR–$R_{496–719}$) (a), reflectance between 648 and 719 nm (SVR–$R_{648–719}$) (b), and continuum removed reflectance of the latter spectral interval without the edging wavelengths gaining zero values (SVR–$CR_{652–715}$) (c). LD was also estimated by support vector regression from samples of 1999 (n = 24) using sample reflectance between 708 and 848 nm (SVR–$R_{708–848}$) (d), reflectance between 708 and 782 nm (SVR–$R_{708–782}$) (e), and continuum removed reflectance of the latter spectral interval without the edging wavelengths gaining zero values (SVR–$CR_{711–778}$) (f). Estimates are plotted against Cab content and LD measured in laboratory. Solid line indicates the expected one-to-one linear relationship and dashed line is the linear regression function computed between measured and estimated Cab (r^2 ~ coefficient of determination, d ~ index of agreement, RMSE ~ root mean square error, $RMSE_S$ ~ systematic component of RMSE, $RMSE_U$ ~ unsystematic component of RMSE).

Fig. 8

Maps of quantitative stress indicators: chlorophyll *a*+*b* content (a), effective moss turf leaf density (b), and a synthetic map of relative moss vigour indicator (c) derived for the *dry* test site of the ASPA 135 *Schistidium antarctici* moss bed from the field hyperspectral image acquired on 10 January 2013 using the best performing support vector regression models trained with moss laboratory measurements. The maps were generalised with a median filter of 7 by 7 pixels for easier interpretation. Grey and black colours represent rocks, bare soil, lichens, and desiccated black moss turf.

Fig. 9

Maps of quantitative stress indicators: chlorophyll *a*+*b* content (a), effective moss turf leaf density (b), and a synthetic map of relative moss vigour indicator (c) derived for the *wet* test site of the ASPA 135 *Schistidium antarctici* moss bed from the field hyperspectral image acquired on 30 January 2013 using the best performing support vector regression models trained with moss laboratory measurements. The maps were generalised with a median filter of 7 by 7 pixels for easier interpretation. Grey and black colours represent rocks, bare soil, lichens, and desiccated black moss turf.

Fig. 10

Frequency histograms displaying relative abundance of chlorophyll *a*+*b* content (Cab) (a, d), effective moss turf leaf density (LD) (b, e), and the relative vigour indicator (RVI) (c, f) integrating both quantitative characteristics for all photosynthetically active moss pixels captured in the hyperspectral scan of the ASPA 135 *dry* test site (a–c, see Fig. 8) and *wet* test site (d–f, see Fig. 9).

Fig. 11

Schematic interactions between shoot structure and photons of near infrared (NIR) light demonstrating the link between turf water content (TWC), effective leaf density (LD) and resulting NIR reflectance. Leaves of hydrated moss are fully expanded (a, c, and d), which means that the upper canopy reflects a significant portion of incident NIR light (up to 50%; e.g. Fig. 6, 25/01/2013). Contrary to this, shoots of desiccated moss are shrunken with curled leaves (b, e, and f), allowing NIR photons to penetrate and be absorbed deeper inside the canopy, which reduces NIR reflectance (sometimes by more than half; e.g. Fig. 6, 01/01/2013). Smaller leaves of higher LD, typical for a moss impacted by a chronic stress (d and f), trigger more interactions between NIR photons and moss shoots (i.e. a higher multiple scattering), which increases the probability of NIR transmission and/or absorption by the canopy. This diminishes the NIR reflection, even when turf is wet and leaves are expanded (d). Upon desiccation, mosses shrink and their leaves curl, which simulates increased shoot LD and produces NIR photon-leaf interactions similar to those inside a moss turf with expanded leaves of a higher density (c.f. c and d vs. e). The desiccation-induced structural changes enhance diffusion and absorbance of NIR light in lower turf layers, which further reduces amount of NIR photons reflected by dry moss gametophytes with small curled leaves of a high LD (f).

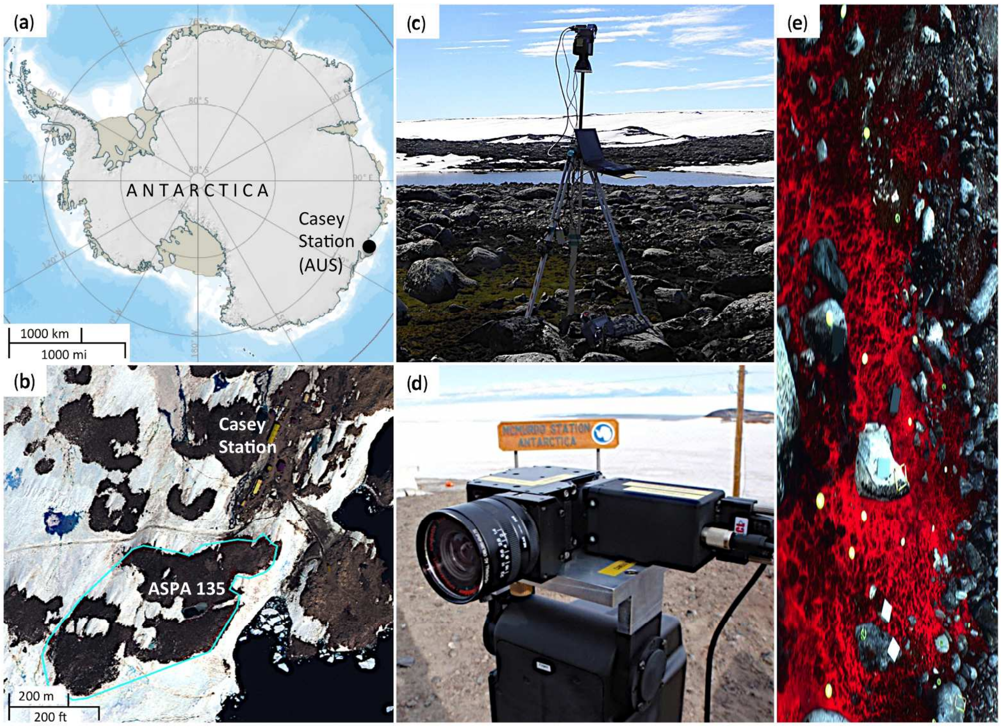

Geographical location of Antarctic Specially Protected Area (ASPA) 135 study sites close to the Australian Antarctic station Casey (a, b); the ground-based hyperspectral instrumentation in field (at the *dry* test site) (c); the Micro-Hyperspec imaging spectroradiometer (Headwall Inc., USA) mounted on rotation and tilt platform (d); and a false-coloured near-distance hyperspectral image of a *Schistidium antarctici* moss bed at the *dry* test site (e). Red colour indicates photosynthetically active mosses, whereas grey and black colours represent rocks, bare soil, lichens, and desiccated black turf.
320x231mm (300 x 300 DPI)

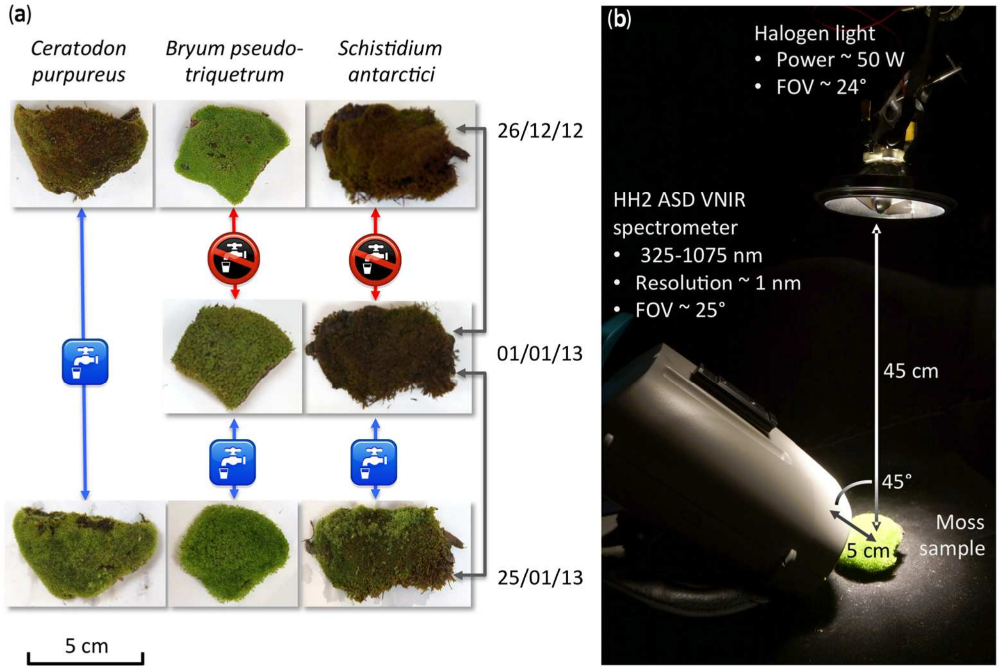

Examples of laboratory drought-stress rehydration experiment samples of the three Antarctic moss species (*Ceratodon purpureus*, *Bryum pseudotriquetrum* and *Schistidium antarctici*) collected on 26 December 2012 (a). Half of the samples serving as controls were kept in optimal growing conditions and irrigated during the whole experiment (see example of red-coloured *C. purpureus*; blue tap icon symbolises regular irrigation every 2nd day), while the other half was kept without water until 1 December 2013 and then irrigated regularly until the end of the experiment on 25 January 2013 (see examples of green *B. pseudotriquetrum* and red-coloured *S. antarctici*; red crossed tap icon symbolises water-stress). Reflectance of all moss samples was measured every 6th day in a dark chamber with an ASD HandHeld-2 (HH2) spectrometer (ASD Inc. & PANalytical, USA) coupled with a halogen tungsten irradiation light source (b).
160x106mm (300 x 300 DPI)

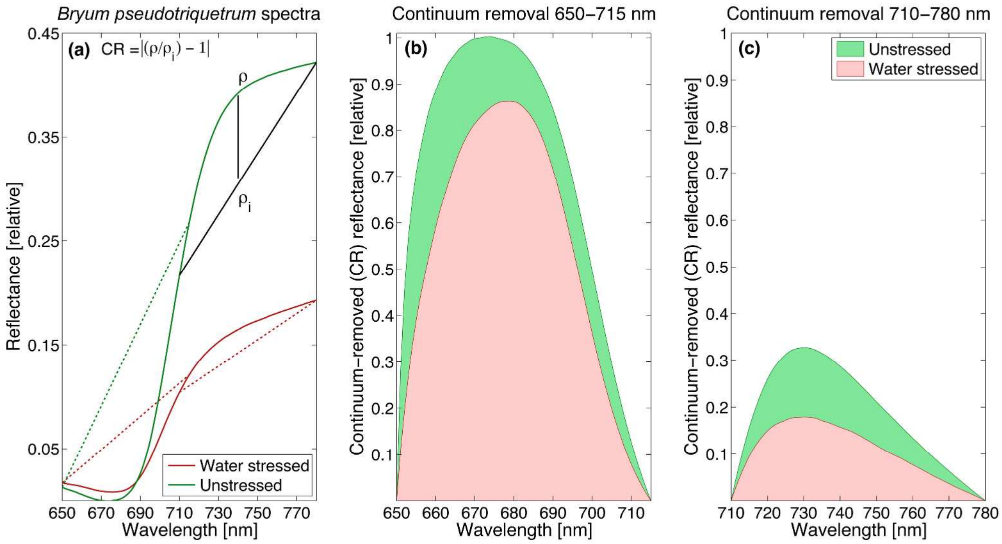

Mathematical explanation of the continuum removal (CR) transformation for spectral ranges of 650–715 and 710–780 nm, demonstrated on reflectance functions of a water-stressed and an unstressed *Bryum pseudotriquetrum* (a). Linearly interpolated values (ρ_i) are first computed for the given spectral intervals (dotted lines) and then applied per wavelength to normalize the original reflectance (ρ). The absolute value of this ratio subtracted from one results in the continuum removed (CR) reflectance of both spectral intervals: 650–715 nm (b) and 710–780 nm (c).
388x212mm (300 x 300 DPI)

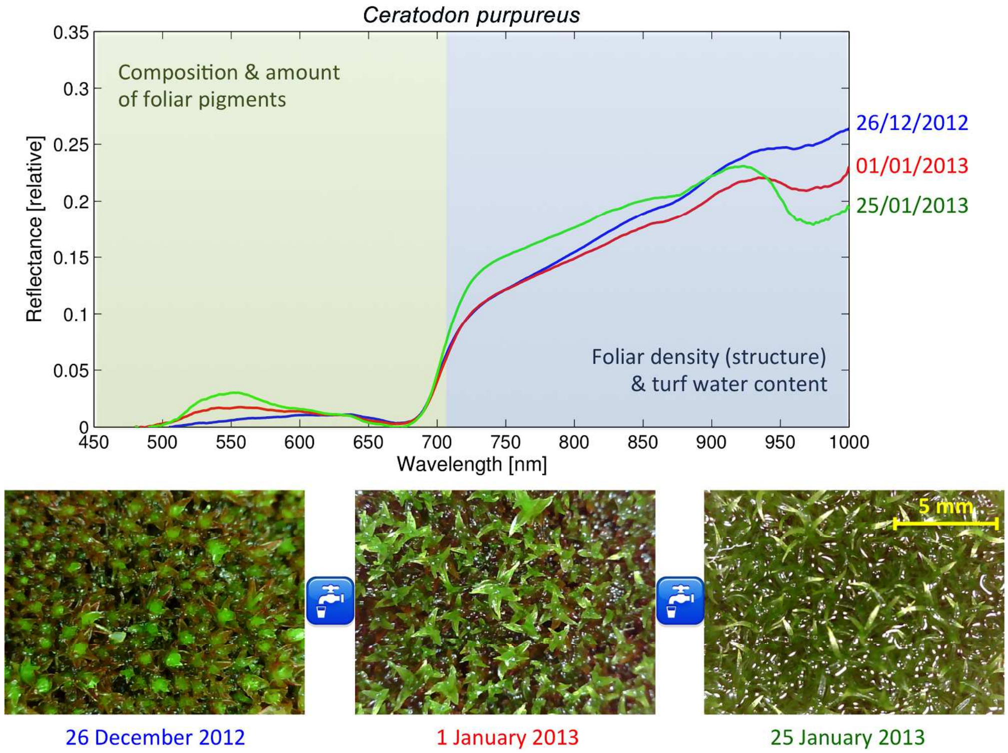

Reflectance signatures and corresponding micro-photographs of *Ceratodon purpureus* collected and measured on 26 December 2012 (MTVI2 = 0.36), kept in optimal growing conditions (sufficiently irrigated) and re-measured on 1 January 2013 (MTVI2 = 0.39) and 25 January 2013 (MTVI2 = 0.67). The green background highlights the spectral range influenced mainly by actual composition and amount of foliar pigments, whereas the blue background indicates the spectral range influenced mainly by effective turf foliar density and actual turf water content.
320x239mm (300 x 300 DPI)

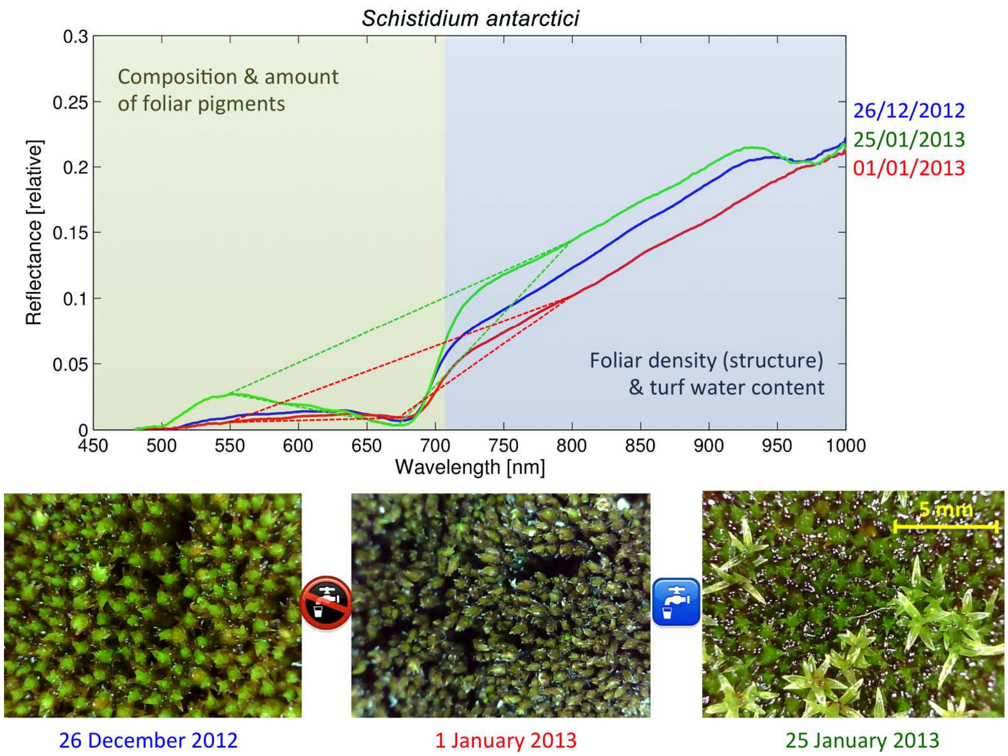

Reflectance signatures and corresponding micro-photographs of *Schistidium antarctici* collected and measured on 26 December 2012 (MTVI2 = 0.26), kept in a growth chamber without water and re-measured on 1 January 2013 (MTVI2 = 0.17), then rehydrated (sufficiently irrigated) and measured again on 25 January 2013 (MTVI2 = 0.39). Dashed lines delineating triangles between reflectance amplitudes at 550, 670 and 800 nm indicate increase in the area inside of the triangle with decreasing stress load. Declining MTVI2, caused by shrinking and curling of leaves indicates low water content on 1 January 2013. Green and blue backgrounds are explained in Fig. 4.
320x239mm (300 x 300 DPI)

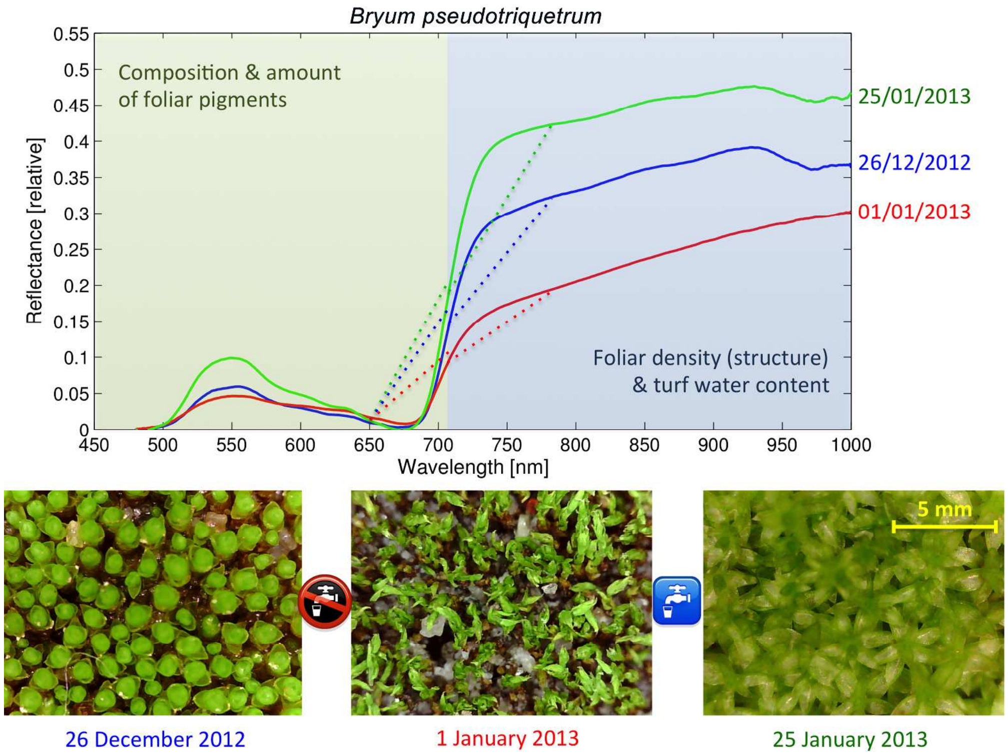

Reflectance signatures and corresponding microscopic photographs of *Bryum pseudotriquetrum* collected and measured on 26 December 2012 (MTVI2 = 0.92), kept in a growth chamber without water and re-measured on 1 January 2013 (MTVI2 = 0.49), and then rehydrated and measured again on 25 January 2013 (MTVI2 = 1.46). Dotted lines denote spectral regions used for the continuum removal transformation. They show that both areas under the curve at 650–715 nm and at 710–780 nm increase as the stress load decreases and as the moss turf produces more chlorophyll and leaves open up. Declining MTVI2, caused by shrinking and curling of leaves and shoots, indicates low water content on 1 January 2013. Green and blue backgrounds are explained in Fig. 4.
320x240mm (300 x 300 DPI)

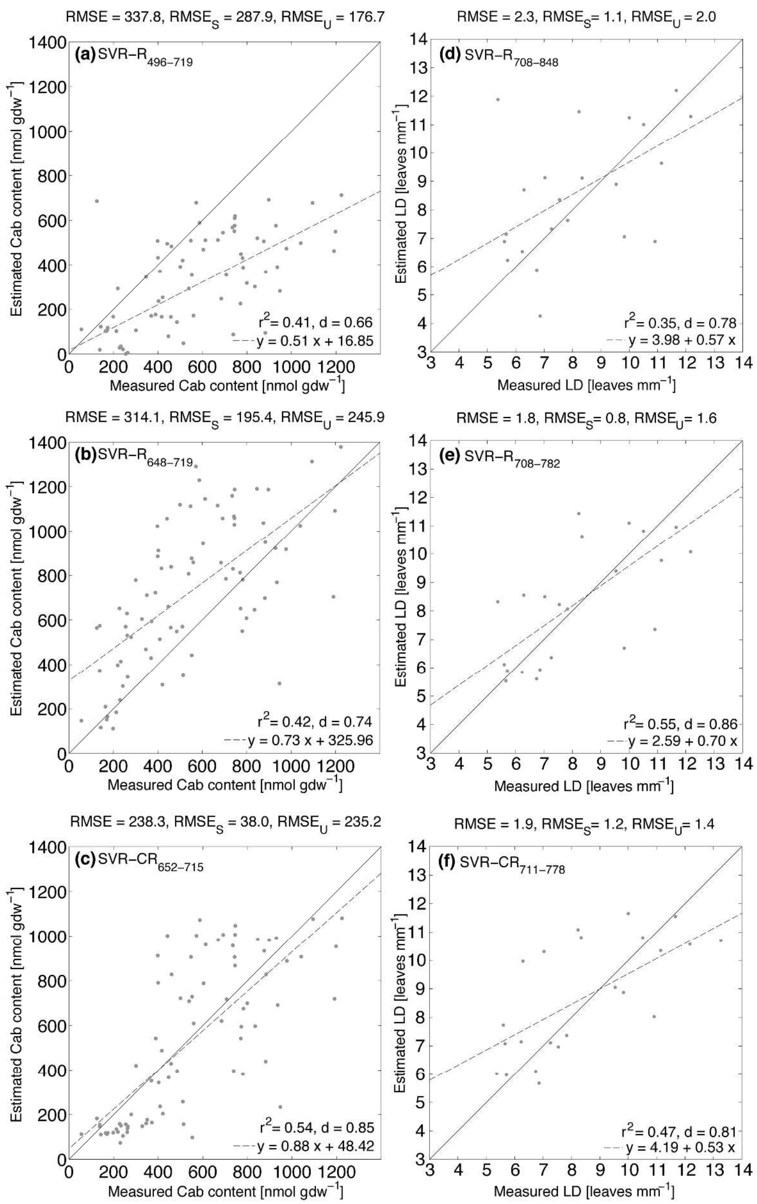

Accuracy assessment of chlorophyll *a+b* content (Cab) and mean leaf density (LD) estimates from *Schistidium antarctici* spectral measurements. Cab was estimated by support vector regression from samples collected in 1999 (n = 80) using their reflectance between 496 and 719 nm (SVR–R$_{496–719}$) (a), reflectance between 648 and 719 nm (SVR–R$_{648–719}$) (b), and continuum removed reflectance of the latter spectral interval without the edging wavelengths gaining zero values (SVR–CR$_{652–715}$) (c). LD was also estimated by support vector regression from samples of 1999 (n = 24) using sample reflectance between 708 and 848 nm (SVR–R$_{708–848}$) (d), reflectance between 708 and 782 nm (SVR–R$_{708–782}$) (e), and continuum removed reflectance of the latter spectral interval without the edging wavelengths gaining zero values (SVR–CR$_{711–778}$) (f). Estimates are plotted against Cab content and LD measured in laboratory. Solid line indicates the expected one-to-one linear relationship and dashed line is the linear regression function computed between measured and estimated Cab (r^2 ~ coefficient of determination, d ~ index of agreement, RMSE ~ root mean square error, RMSE$_S$ ~ systematic component of RMSE, RMSE$_U$ ~ unsystematic component of RMSE).

283x450mm (300 x 300 DPI)

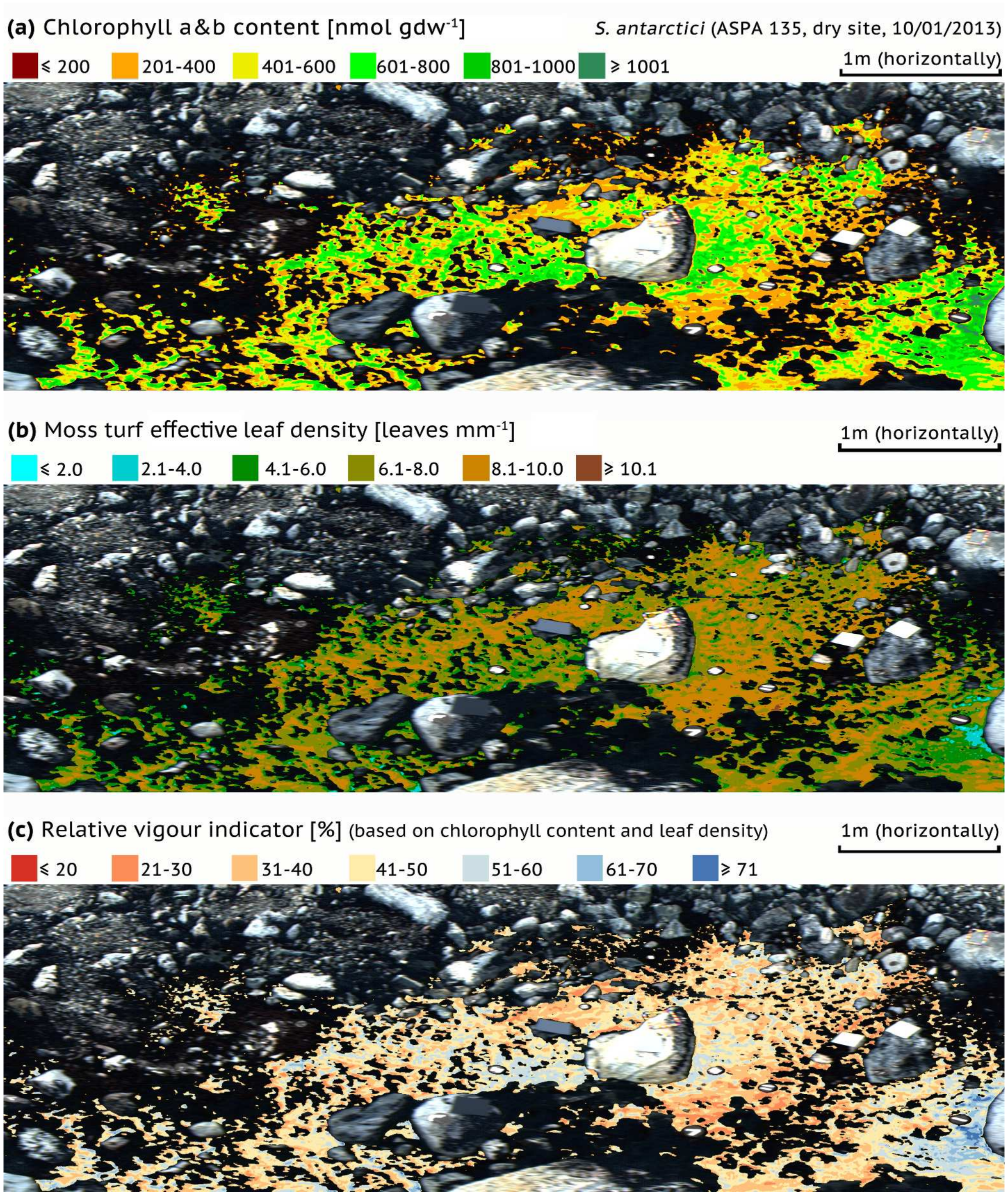

Maps of quantitative stress indicators: chlorophyll *a+b* content (a), effective moss turf leaf density (b), and a synthetic map of relative moss vigour indicator (c) derived for the *dry* test site of the ASPA 135 *Schistidium antarctici* moss bed from the field hyperspectral image acquired on 10 January 2013 using the best performing support vector regression models trained with moss laboratory measurements. The maps were generalised with a median filter of 7 by 7 pixels for easier interpretation. Grey and black colours represent rocks, bare soil, lichens, and desiccated black moss turf.
279x331mm (300 x 300 DPI)

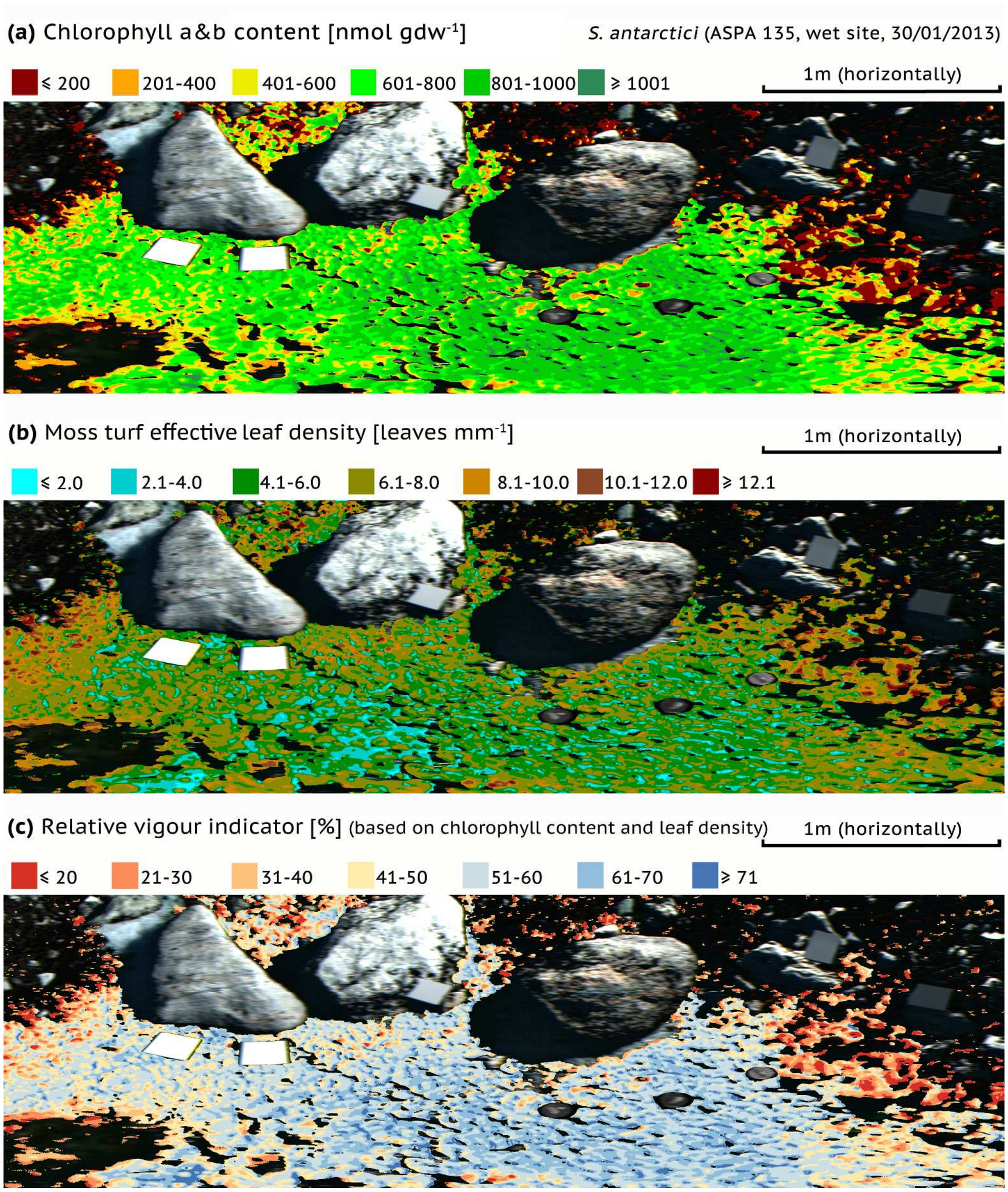

Maps of quantitative stress indicators: chlorophyll *a+b* content (a), effective moss turf leaf density (b), and a synthetic map of relative moss vigour indicator (c) derived for the *wet* test site of the ASPA 135 *Schistidium antarctici* moss bed from the field hyperspectral image acquired on 30 January 2013 using the best performing support vector regression models trained with moss laboratory measurements. The maps were generalised with a median filter of 7 by 7 pixels for easier interpretation. Grey and black colours represent rocks, bare soil, lichens, and desiccated black moss turf.
279x330mm (300 x 300 DPI)

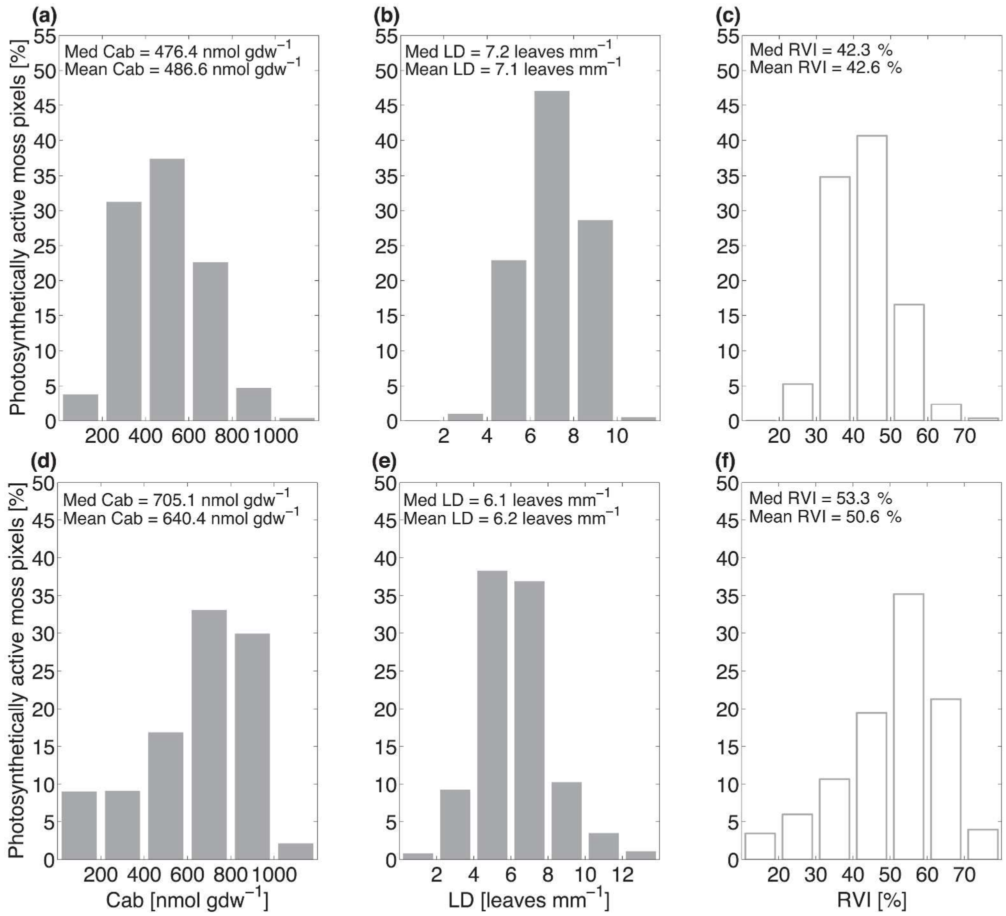

Frequency histograms displaying relative abundance of chlorophyll *a+b* content (Cab) (a, d), effective moss turf leaf density (LD) (b, e), and the relative vigour indicator (RVI) (c, f) integrating both quantitative characteristics for all photosynthetically active moss pixels captured in the hyperspectral scan of the ASPA 135 *dry* test site (a–c, see Fig. 8) and *wet* test site (d–f, see Fig. 9).
407x372mm (300 x 300 DPI)

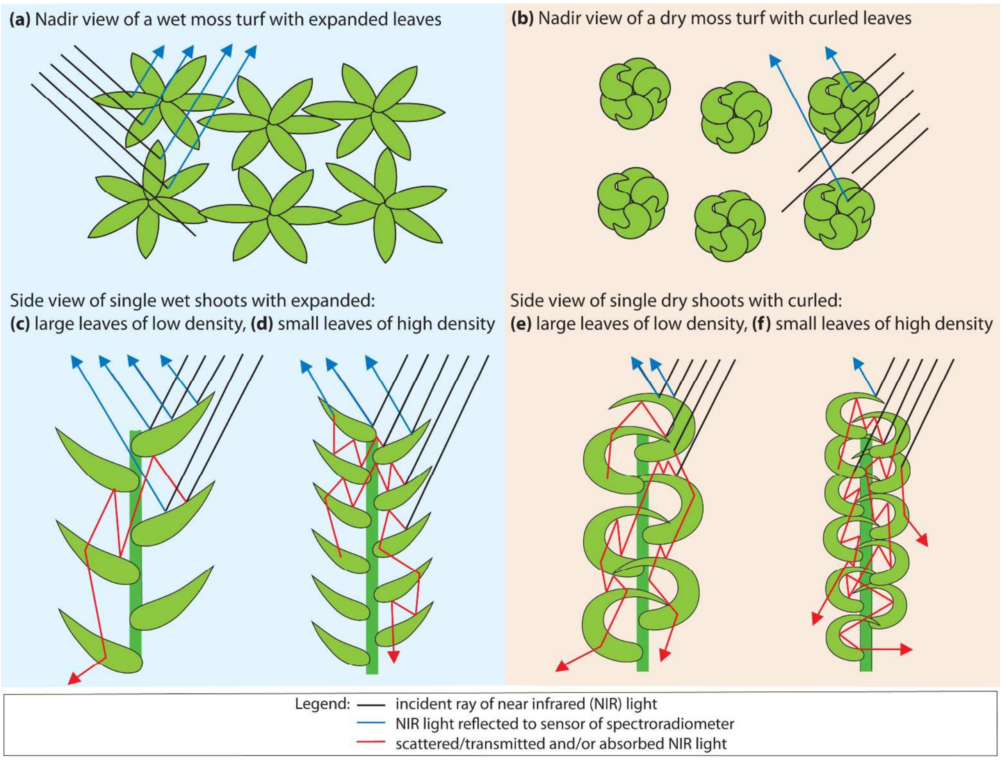

Schematic interactions between shoot structure and photons of near infrared (NIR) light demonstrating the link between turf water content (TWC), effective leaf density (LD) and resulting NIR reflectance. Leaves of hydrated moss are fully expanded (a, c, and d), which means that the upper canopy reflects a significant portion of incident NIR light (up to 50%; e.g. Fig. 6, 25/01/2013). Contrary to this, shoots of desiccated moss are shrunken with curled leaves (b, e, and f), allowing NIR photons to penetrate and be absorbed deeper inside the canopy, which reduces NIR reflectance (sometimes by more than half; e.g. Fig. 6, 01/01/2013). Smaller leaves of higher LD, typical for a moss impacted by a chronic stress (d and f), trigger more interactions between NIR photons and moss shoots (i.e. a higher multiple scattering), which increases the probability of NIR transmission and/or absorption by the canopy. This diminishes the NIR reflection, even when turf is wet and leaves are expanded (d). Upon desiccation, mosses shrink and their leaves curl, which simulates increased shoot LD and produces NIR photon-leaf interactions similar to those inside a moss turf with expanded leaves of a higher density (c.f. c and d vs. e). The desiccation-induced structural changes enhance diffusion and absorbance of NIR light in lower turf layers, which further reduces amount of NIR photons reflected by dry moss gametophytes with small curled leaves of a high LD (f).
277x209mm (300 x 300 DPI)

***New Phytologist* Supporting Information**

Article title: **Antarctic moss stress assessment based on chlorophyll, water content, and leaf density retrieved from imaging spectroscopy data**

Authors: Zbyněk Malenovský, Johanna D. Turnbull, Arko Lucieer, Sharon A. Robinson

Article acceptance date: 17 May 2015

The following Supporting Information is available for this article:

Fig. S1 Illustration of *dry* and *wet* research plots at the Antarctic Specially Protected Area 135.

Fig. S2 Establishment of the modified triangular vegetation index 2 (MTVI2) threshold.

Fig. **S3** Spectral quality validation of ground-based hyperspectral images acquired at both plots.

Table S1 Optimised input parameters and mean square errors of support vector regressions.

Fig. S1 Photographs of *dry* (whole season exposed, water limited, and considerably stressed) site (a) and *wet* (lengthily snow covered, well watered, and less stressed) research site (b) at the Antarctic Specially Protected Area 135 (ASPA 135) colonized predominantly by moss *Schistidium antarctici*.

Fig. S2 Establishment of the modified triangular vegetation index 2 (MTVI2) threshold separating rocks, bare soil, and desiccated dormant moss from the photosynthetically active moss using frequency histograms of all pixels recorded in hyperspectral images of the ASPA 135 *dry* (a) and *wet* (b) test sites. Dashed lines indicate the actual MTVI2 threshold of 0.25.

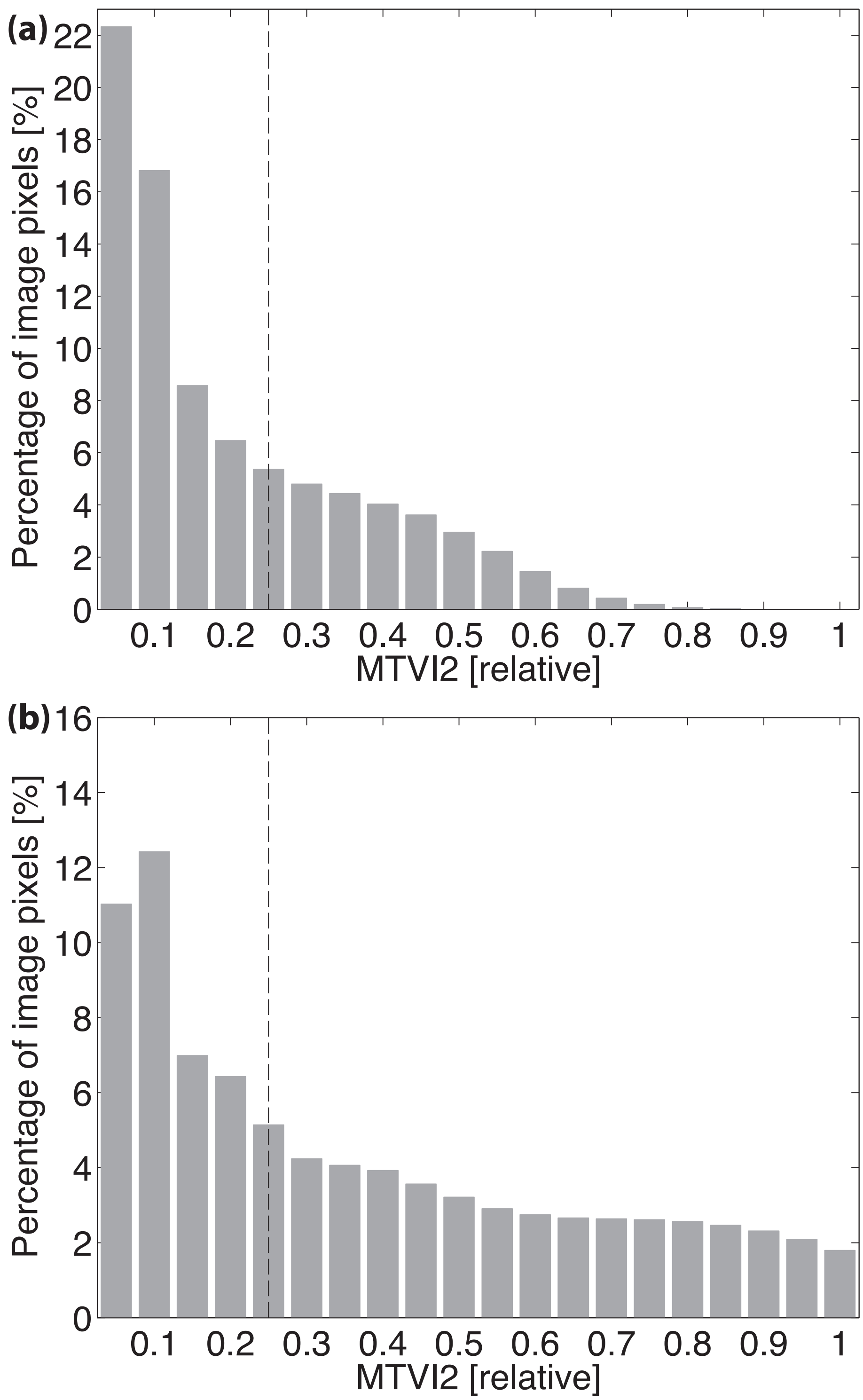

Fig. S3 Spectral quality validation of hyperspectral reflectance acquired with the ground-based Micro-Hyperspec imaging spectroradiometer (Headwall Inc., Fitchburg, USA) for two study plots in the vicinity of the Australian Antarctic station Casey during the summer 2012–2013. Mean ground-based reflectance signatures (± SD, n = 3, black lines) collected with the ASD HandHeld-2 spectrometer (ASD Inc. & PANalytical, Boulder, USA) for dark (a), medium bright (b), and bright stones (c), plus green moss (d) surfaces are plotted over the mean reflectance (± SD) computed from 49 image pixels of the same targets located in the hyperspectral images (white and grey lines) (r^2 ~ coefficient of determination for established linear regression, RMSE ~ root mean square error, and d ~ index of agreement between target reflectance of all wavelengths).

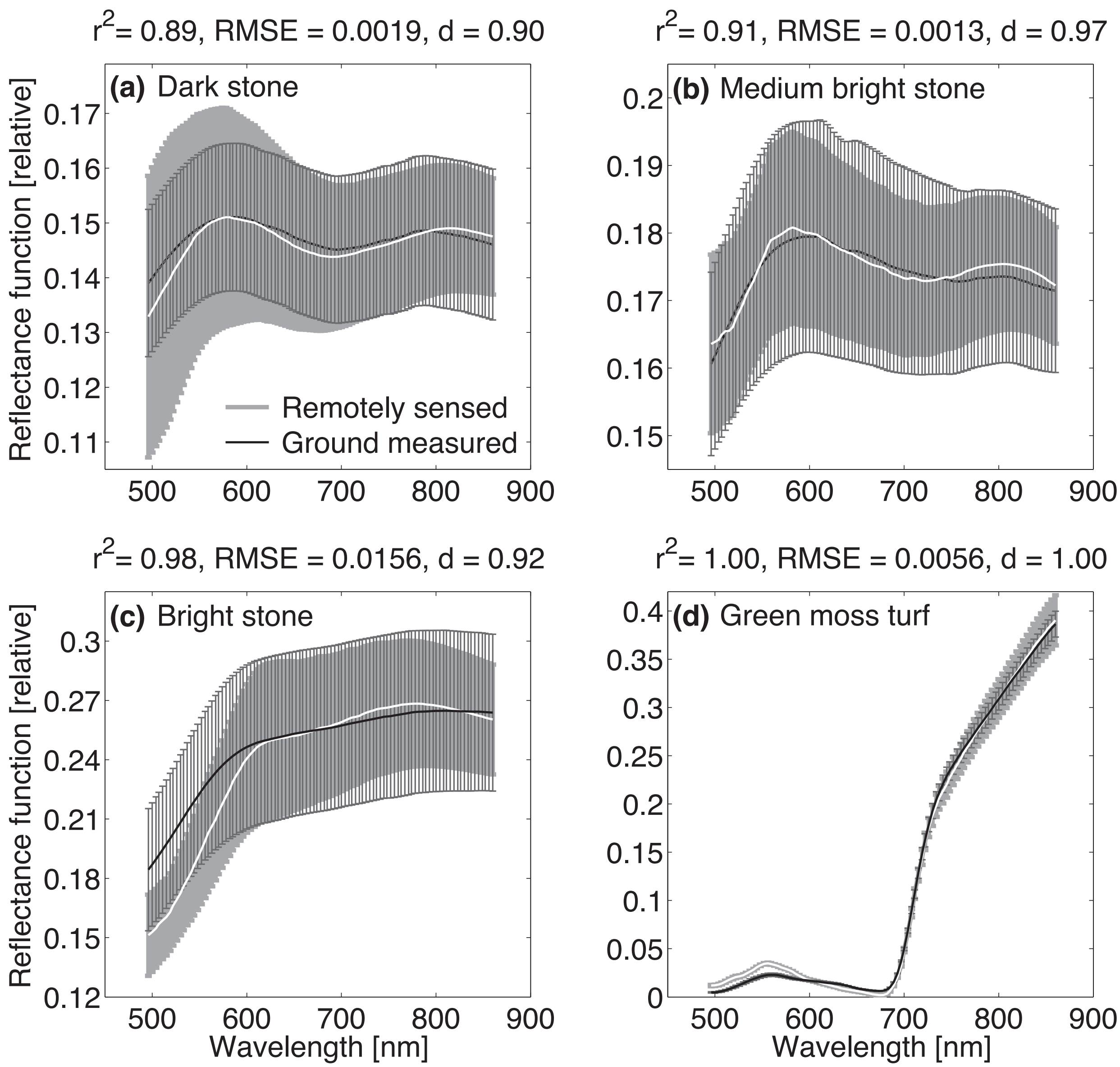

Table S1 Optimised cost and kernel width parameters, with affiliated mean square errors (MSE) of the epsilon support vector regression (SVR) models trained for estimation of chlorophyll a+b (Cab), turf water content (TWC), and leaf density (LD) using moss reflectance (R) and continuum removed reflectance (CR) of four investigated spectral regions: 498–719, 648–719, 708–848, and 708–782 nm.

Model	*Cost parameter C*	*Kernel width γ*	*Mean square error*
Cab			
SVR–$R_{496–719\ nm}$	1048576	0.00003	4.2608
SVR–$R_{648–719\ nm}$	32768	0.00780	4.3767
SVR–$CR_{496–719\ nm}$	1024	0.01560	3.9337
TWC			
SVR–$R_{708–848\ nm}$	8192	0.00390	3.2173
SVR–$R_{708–782\ nm}$	512	0.00780	2.2979
SVR–$CR_{708–782\ nm}$	4096	0.03130	3.7921
LD			
SVR–$R_{708–848\ nm}$	32768	0.00200	3.3243
SVR–$R_{708–782\ nm}$	16384	0.00390	3.5814
SVR–$CR_{708–782\ nm}$	4	0.12500	3.0493